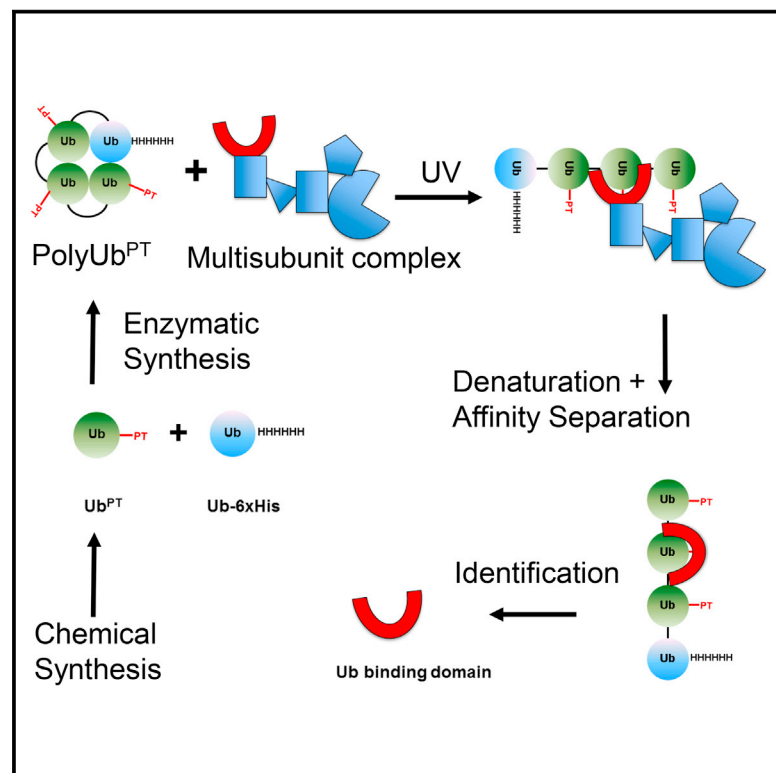


Cell Chemical Biology

Polyubiquitin-Photoactivatable Crosslinking Reagents for Mapping Ubiquitin Interactome Identify Rpn1 as a Proteasome Ubiquitin-Associating Subunit

Graphical Abstract



Authors

Michal Chojnacki, Wissam Mansour, Dharjath S. Hameed, ..., David Fushman, Huib Ovaa, Michael H. Glickman

Correspondence

fushman@umd.edu (D.F.), h.ovaa@lumc.nl (H.O.), glickman@tx.technion.ac.il (M.H.G.)

In Brief

Application of polyubiquitin-phototrap (polyUb^{PT}), a novel set of chain-specific inducible photo-crosslinking probes, enables trapping of transient partners through the hydrophobic patch of ubiquitin. PolyUb^{PT} captured Rpn1 from intact proteasome complexes. Rpn1 joins Rpn10 and Rpn13 as a proteasome subunit with affinity for polyUb and Ub-like domains.

Highlights

- Photoleucine was successfully incorporated into fully synthetic ubiquitin monomers
- Embedded photoleucine permitted binding to the hydrophobic patch of ubiquitin
- Enzymatically polymerized ubiquitin phototrap captured Ub-binding receptors
- The first PC region of Rpn1, either isolated or proteasome-incorporated, bound polyUb



Polyubiquitin-Photoactivatable Crosslinking Reagents for Mapping Ubiquitin Interactome Identify Rpn1 as a Proteasome Ubiquitin-Associating Subunit

Michal Chojnacki,^{1,2,9} Wissam Mansour,^{1,9} Dharjath S. Hameed,^{3,8} Rajesh K. Singh,⁴ Farid El Oualid,^{3,10} Rina Rosenzweig,^{5,7} Mark A. Nakasone,¹ Zanlin Yu,¹ Fabian Glaser,⁶ Lewis E. Kay,⁵ David Fushman,^{4,*} Huib Ovaa,^{3,8,*} and Michael H. Glickman^{1,11,*}

¹Department of Biology, Technion-Israel Institute of Technology, 32000 Haifa, Israel

²Department of Medical Biochemistry, Medical University of Łódź, Łódź, Poland

³Division of Cell Biology, The Netherlands Cancer Institute, Plesmanlaan 121, 1066 CX Amsterdam, the Netherlands

⁴Department of Chemistry and Biochemistry, Center for Biomolecular Structure and Organization, University of Maryland, College Park, MD 20742, USA

⁵Departments of Molecular Genetics, Biochemistry and Chemistry, The University of Toronto, Toronto, ON M5S 1A8, Canada

⁶The Technion Bioinformatics Knowledge Unit (BKU) of the Lorry Lokey Interdisciplinary Center for Life Sciences and Engineering, Technion-Israel Institute of Technology, 32000 Haifa, Israel

⁷Department of Structural Biology, Weizmann Institute of Science, Rehovot 7610001, Israel

⁸Department of Chemical Immunology, Leiden University Medical Center, Einthovenweg 20, 2333 ZC Leiden, the Netherlands

⁹Co-first author

¹⁰Present address: UbiQ Bio BV, Science Park 408, 1098 XH Amsterdam, the Netherlands

¹¹Lead Contact

*Correspondence: fushman@umd.edu (D.F.), h.ovaa@lumc.nl (H.O.), gllickman@tx.technion.ac.il (M.H.G.)

<http://dx.doi.org/10.1016/j.chembiol.2017.02.013>

SUMMARY

Ubiquitin (Ub) signaling is a diverse group of processes controlled by covalent attachment of small protein Ub and polyUb chains to a range of cellular protein targets. The best documented Ub signaling pathway is the one that delivers polyUb proteins to the 26S proteasome for degradation. However, studies of molecular interactions involved in this process have been hampered by the transient and hydrophobic nature of these interactions and the lack of tools to study them. Here, we develop Ub-phototrap (Ub^{PT}), a synthetic Ub variant containing a photoactivatable crosslinking side chain. Enzymatic polymerization into chains of defined lengths and linkage types provided a set of reagents that led to identification of Rpn1 as a third proteasome ubiquitin-associating subunit that coordinates docking of substrate shuttles, unloading of substrates, and anchoring of polyUb conjugates. Our work demonstrates the value of Ub^{PT}, and we expect that its future uses will help define and investigate the ubiquitin interactome.

INTRODUCTION

Myriad intracellular processes in eukaryotes are directed through ubiquitin (Ub) signaling (Glickman and Ciechanover, 2002; Hershko and Ciechanover, 1998). The versatility of Ub signaling is largely due to the numerous ways in which individual

Ub units can be assembled into polymers. Forming an isopeptide bond, the C terminus of one Ub module links the ϵ -amine residue of a lysine side chain of another in poly-ubiquitin (polyUb) chains. Eight different linkages in polyUb chains include conjugation at the seven-lysine side chains on each Ub molecule (K6, K11, K27, K29, K33, K48, and K63) and elongation through the N terminus of Ub. In a similar manner, polyUb chains are attached either to a lysine residue or to the N terminus of a target protein. The linkage type and length of the polyUb signal determines the fate of the conjugated target; for example, K48 linkages are the canonical signal for degradation by proteasomes, whereas K63-linked chains are involved in non-degradative pathways (e.g., intracellular sorting, membrane-associated trafficking, or DNA damage response). The outcome often requires Ub-binding proteins that interpret each specific signal. Ub-binding domains (UBDs) span several distinct protein families and are broadly distributed throughout the cell (Husnjak and Dikic, 2012; Rahighi and Dikic, 2012; Scott et al., 2015). Most UBDs show a marked preference for polyUb chains over monoUb, and in some cases recognition is linkage specific (Fushman and Wilkinson, 2011; Hofmann, 2009; Hurley et al., 2006; Raasi et al., 2005; Sims and Cohen, 2009). For instance, one important class of Ub-binding proteins shuttles polyUb conjugates, primarily K48-linked, from various cellular locations to proteasome complexes, where they are degraded. As molecular mediators, association of UBDs with polyUb tends to be transient in order to facilitate relay of cargo at its final destination. Capturing these relatively intermediate-strength interactions is an experimental challenge.

The 26S proteasome, a 2.5 MDa multisubunit complex composed of a proteolytic 20S core particle (CP) and a 19S regulatory particle (RP), is the final destination for many polyUb-tagged cellular proteins (Mayor et al., 2016). Two proteasome subunits, Rpn10 and Rpn13 (recently joined by Rpn1;

Shi et al., 2016), are established polyUb receptors and are thought to serve as docking sites for polyUb conjugates. In addition, a number of transiently proteasome-associated shuttle proteins facilitate degradation by targeting Ub conjugates to proteasomes. The bivalent shuttles capture polyUb by means of a ubiquitin-associated (UBA) domain and simultaneously dock at the 19S RP via a ubiquitin-like (UBL) domain. Although UBL domains associate with Rpn1 at the proteasome, docking of these shuttles may partially overlap with the site of direct polyUb binding since Rpn10 and Rpn13 display affinity for UBLs as well as for polyUb (Elsasser et al., 2002, 2004; Fatimababy et al., 2010; Hamazaki et al., 2015; Husnjak et al., 2008; Kim et al., 2004; Matiuhin et al., 2008; Rosenzweig et al., 2012; Sakata et al., 2012; Schreiner et al., 2008; Zhang et al., 2009b). Once anchored, the hexameric ring of AAA-ATPases resident in the 19S RP (Rpt1–6) unfolds the substrate and promotes translocation into the proteolytic core of the 20S CP (Schweitzer et al., 2016). In parallel, proteasome-associated deubiquitinases (DUBs) remove the polyUb signal from the substrate (Finley, 2009; Glickman and Adir, 2004; Guterman and Glickman, 2004; Lee et al., 2011; Mansour et al., 2015). DUB and ATPase activities are carefully coordinated in the 19S RP to allow for proteolytic efficiency and recycling of Ub (Aufderheide et al., 2015; Matyskiela et al., 2013; Peth et al., 2009, 2013a, 2013b; Singh et al., 2016; Verma et al., 2000, 2002). These activities are coordinated, to a large extent, by the two largest subunits in the 19S RP, Rpn1 and Rpn2, that function as flexible scaffolds. Both proteins contain a central domain of multiple alpha-turn-alpha proteasome/cyclosome (PC) repeats that fold into structurally similar highly curved toroids, extended by divergent flexible N- and C-terminal regions (Effantin et al., 2009; He et al., 2012; Kajava, 2002; Rosenzweig et al., 2012). Although Rpn1 and Rpn2 share much in common structurally (Effantin et al., 2009; He et al., 2012; Lander et al., 2012; Unverdorben et al., 2014), their different positions within the 19S RP and different binding partners make them fascinating candidates for functional analysis.

Rpn1 associates with UBL domains found in auxiliary proteins Rad23/hHR23, Dsk2/hPLIC/Ubiquilin, Ddi1, and Ubp6/USP14, all of which also contain a domain with high affinity for polyUb (Aufderheide et al., 2015; Elsasser et al., 2002; Kim et al., 2004; Nowicka et al., 2015; Peth et al., 2009, 2013a; Rosenzweig et al., 2012). The paralog subunit, Rpn2, has been shown to form tight interactions with the polyUb receptor Rpn13/ADRM1, and with the proteasome-associated DUB, UCH37/UCH-L5 (Aufderheide et al., 2015; Bashore et al., 2015; Hamazaki et al., 2006; He et al., 2012; Sakata et al., 2012). Determining how proteasome recognizes and processes substrates is the subject of intense research efforts. Beyond K48-linked polyUb modifications that have long been considered the primary proteasome targeting signal, a diverse range of polyUb signals can apparently be recognized by the proteasome (Lu et al., 2015; Mansour et al., 2015; Meyer and Rape, 2014; Nathan et al., 2013; Saeki et al., 2009). The limited binding capacity of Rpn10 and Rpn13, and the fact that they are not essential for viability of *Saccharomyces cerevisiae*, indicate that additional proteasomal subunits interact either directly with polyUb or with shuttle factors that aid targeting. In fact, a report suggests that Ubp6, as a rather slow-acting DUB, is a principal proteasomal polyUb receptor (Peth et al., 2009). Thus, Ubp6, a transiently associating proteasomal

subunit, has been reported to double up as an anchor for polyUb conjugates (Aufderheide et al., 2015; Peth et al., 2009). In contrast, Rpn11, a tightly incorporated proteasomal DUB, has a weak binding affinity for polyUb, raising the possibility that neighboring subunits bind and present polyUb to its catalytic site (Mansour et al., 2015; Pathare et al., 2014; Unverdorben et al., 2014; Worden et al., 2014; Yu et al., 2015). The relatively transient nature of polyUb binding coupled with many potential binding partners and ATP-dependent conformational changes upon substrate engagement (Beckwith et al., 2013; Matyskiela et al., 2013; Sledz et al., 2013b; Unverdorben et al., 2014) pose experimental challenges to track the trajectory of polyUb at proteasomes. The hydrophobic nature of most polyUb recognition events restricts application of many crosslinking approaches, typically modification of polar groups (i.e., crosslinking amine residues and thiols).

In this study, we introduce Ub-phototrap (Ub^{PT}), a variant of Ub in which native leucine residues at a position of choice are replaced by a photoactivatable crosslinking leucine mimic, photoleucine (pLeu). By using linear total chemical synthesis of the 76 amino acid Ub polypeptide, pLeu was introduced at position 8 or 73 in the Ub sequence with high efficiency. The resulting Ub^{PT} is recognized and activated by ubiquitination enzymes and is smoothly incorporated into homogeneously linked polyUb chains (i.e., K48 and K63) of desired length. Next, these conjugates prove to be specifically recognized by UBDs and to be disassembled by DUBs. We validated the use of polyUb^{PT} on intact 26S proteasome complexes in trapping Rpn10 and Rpn13. We then identified Rpn1 as a third proteasome Ub-associating subunit by applying polyUb^{PT}. With isolated Rpn1, the binding region on Rpn1 was narrowed down to the first PC repeat cluster. Nuclear magnetic resonance (NMR) experiments demonstrated that monoUb and polyUb bind Rpn1 through the canonical hydrophobic patch (formed by L8, I44, V70). Competition experiments demonstrated that binding of UBL domains from shuttling factors partially overlaps with binding of polyUb to Rpn1. We conclude that pLeu is a modular and versatile reagent with a unique ability to trap, irreversibly, protein-protein interactions of a hydrophobic nature. Due to these properties, polyUb^{PT} is particularly useful for studying Ub-associating proteins in complex or in isolation.

RESULTS

Chemical Synthesis of Ub^{PT} and a Hybrid Approach for the Generation of PolyUb^{PT} Reagents

Ub-phototrap (Ub^{PT}) was prepared in a linear fashion by solid-phase peptide synthesis as reported earlier (El Oualid et al., 2010) (see Supplemental Information and Schemes S1–S10 for the general protocol and details of the chemical synthesis). Here, the stepwise elongation of the Ub polypeptide is facilitated by the use of pseudoproline and dimethoxybenzyl dipeptides (by preventing the formation of folded and/or aggregated intermediates on resin). The required Fmoc protected photoleucine building block (Janz et al., 2011) was prepared from commercially available L-photoleucine (Figure 1A) and incorporated into the Ub sequence (Zhou et al., 2016). After global deprotection of the synthetic Ub with 90% trifluoroacetic acid (TFA)

followed reversed phase high-performance liquid chromatography (HPLC), pure Ub^{PT} was obtained in 20%–25% overall yield.

Provided that the photoleucine residue (pLeu) is in close proximity to another protein, there are multiple ways for crosslinking to occur, allowing it to be a potent crosslinker (Figure 1B). Following photoactivation, the reactive singlet carbene on the alkyl side chain of pLeu can bond covalently with a number of common functional groups in proteins, thereby increasing the likelihood of trapping binding partners. However, as hydroxyl groups are also prevalent in aqueous environments, the effective chemical half-life of the reactive singlet carbene on exposed or unattached pLeu is short; the trap is essentially self-limiting due to quenching by water. This property decreases crosslinking to spurious proteins thereby increasing the specificity of pLeu embedded in a protein to trap specific binding partners. To expand the use of Ub^{PT}, monomeric Ub molecules in which leucine either at position 8 or 73 was replaced by pLeu, Ub^{PT(8)} and Ub^{PT(73)}, respectively, were ligated enzymatically into homogeneous K48- or K63-linked polyUb chains of defined length with efficiencies comparable with unmodified Ub (Figures 1C and 1D). Here, we refer to poly-Ub^{PT} variants according to their linkage type, chain length, and position of photoleucine: K48-Ub₂^{PT(8)}, K48-Ub₂^{PT(73)}, K48-Ub₄^{PT(8)}, K48-Ub₄^{PT(73)}, K63-Ub₂^{PT(8)}, K63-Ub₂^{PT(73)}, K63-Ub₄^{PT(8)}, and K63-Ub₄^{PT(73)}. Mixing Ub^{PT} with natural, tagged, or mutated Ub and careful choice of E2 Ub conjugation enzymes allows polymerization of chains of modular compositions for use as highly adaptable tools (e.g., for monitoring association with distal versus proximal Ub units in a chain). For instance, by enzymatically polymerizing Ub^{PT} onto a proximal Ub^{6xHis} module, we designed a scheme that allows the isolation of individual Ub-binding subunits from multi-domain complexes after crosslinking under denaturing conditions (Figure 1E).

PolyUb^{PT} Traps PolyUb-Binding Proteins

Linkage-selective antibodies recognized homogeneous K48-linked or K63-linked diUb polymerized from Ub^{PT(8)} or Ub^{PT(73)} with similar efficiency to dimers from unmodified wild-type Ub (Figure 1D). This encouraging observation indicated that polyUb^{PT} could be used to trap linkage-specific Ub-binding proteins. We confirmed the ability of polyUb^{PT} to crosslink proteasome-associated polyUb shuttles and polyUb receptors. For this purpose, we chose dual-function proteins known to function both independently and at the proteasome: Rad23, Dsk2, and Rpn10. The first two are representatives of the UBL-UBA family of shuttle proteins (Diaz-Martinez et al., 2006; Hofmann and Bucher, 1996; Lowe et al., 2006; Ohno et al., 2005; Raasi et al., 2004; Wilkinson et al., 2001; Zhang et al., 2008), whereas Rpn10 is a Ub-interacting motif (UIM)-containing receptor (Matiuhin et al., 2008; Riedinger et al., 2010). Recombinant Rad23, Dsk2, and Rpn10 crosslinked to both Ub₂^{PT(8)} and Ub₂^{PT(73)} of either K48 or K63 linkage type with varying efficiencies, depending on the particular Ub-binding protein (Figure 2A). This is a notable observation given that all three aid proteasome function by shuttling Ub conjugates. Thus, Dsk2 was able to crosslink with both K48- and K63-linked polyUb chains in agreement with our earlier results that the human ortholog, ubiquilin-1, binds both linkage types comparably (Raasi et al., 2004; Sims et al., 2009; Zhang et al., 2008), although

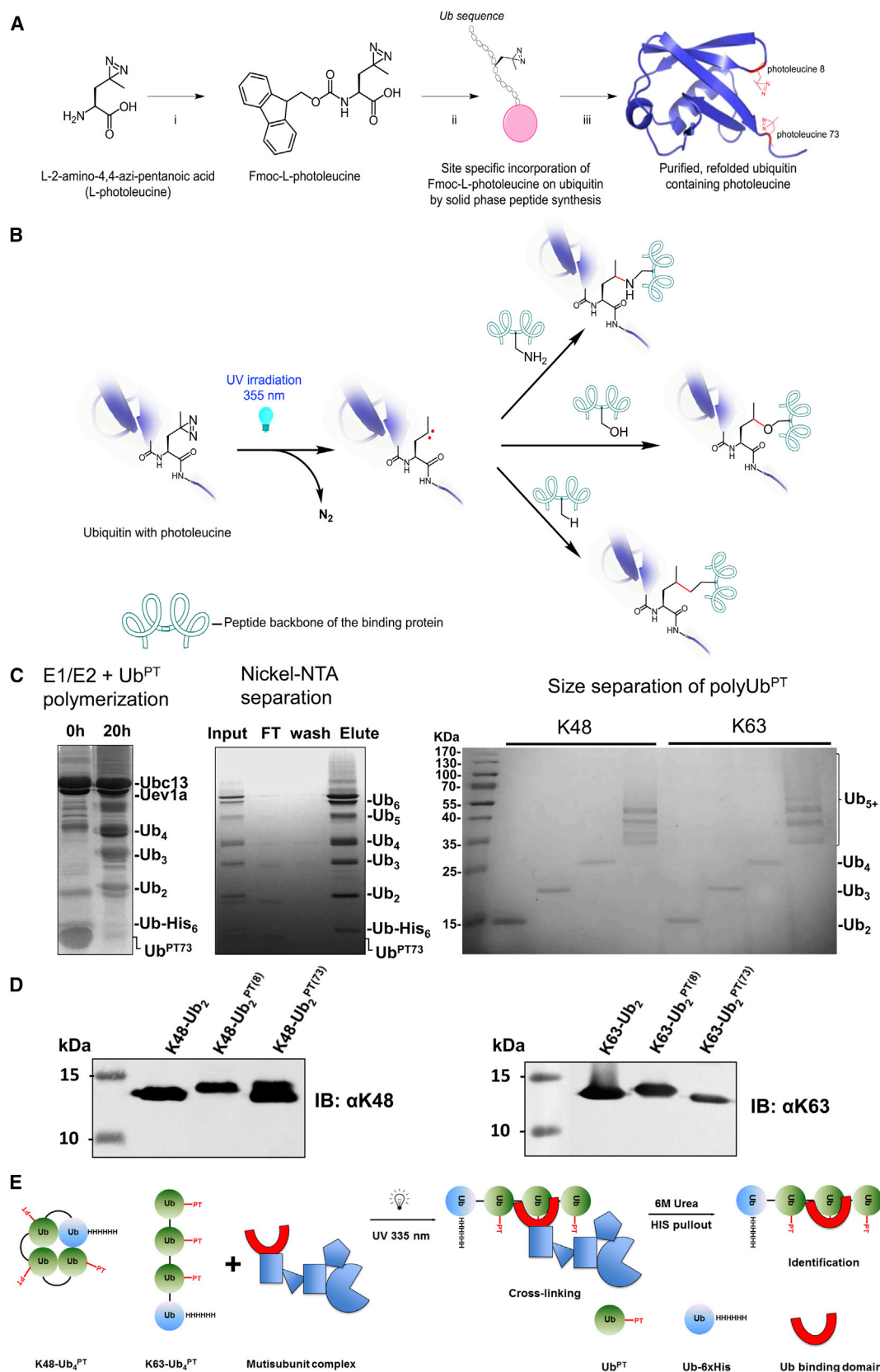
in the current experiment it did display mildly higher efficiency when pLeu was located at position 73 of the Ub signal (Figure 2A). Likewise, Rad23 showed a marked preference for K48-Ub₂^{PT(73)} over K63-linked diUb, consistent with published reports of K48-linkage specificity of UBA1 and UBA2 polyUb-binding domains of the mammalian ortholog hHR23 (Raasi et al., 2004; Varadan et al., 2005). The molecular structure of UBA2 in complex with K48-Ub₂ highlights the proximity of leucine residues 73 and 8 to the UBA binding surface (Figure 2B). In agreement with expectations based on earlier reports (Girod et al., 1999; Matiuhin et al., 2008; Miller et al., 2004; Zhang et al., 2009a, 2009b), Rpn10 also crosslinked to either linkage type, albeit more efficiently to Ub₂^{PT(8)} than to Ub₂^{PT(73)}, alluding to the residues they contact on the surface of Ub. This property probably reflects the orientation of Ub in association with UBA or UIM domains of binding proteins (Hurley et al., 2006). No cross-linked product was detected with Rpn12, a proteasome subunit that served as a negative control, supporting the specificity of polyUb^{PT} for trapping Ub-associating proteins (Figure 2A).

Through work with both ubiquitination enzymes and polyUb shuttles, we demonstrated that alteration of the environment or the nature of the interactions by this replacement is minimal and readily recapitulates known behaviors of unmodified proteins. Use of pLeu has proven successful to map intra-complex interactions in cis, by demonstrating that pre-attached Ub on histone H2B comes in contact with the N terminus of histone H2A (Zhou et al., 2016). By replacing one of the leucine residues involved in binding of Ub to many receptors or shuttles, we show here that pLeu provides an unrivaled tool to study transient hydrophobic associations typical of Ub and polyUb chains.

RAP80, an extensively studied UIM-containing protein, is a polyUb-binding protein that participates in DNA repair presumably unrelated to proteasome function (Wang et al., 2007). RAP80 has been documented to associate selectively with K63-linked polyUb (the binding affinity of the RAP80 tandem ubiquitin interacting motif [tUIM] to K63-Ub₂ or K48-Ub₂ is reported to be $K_D = 21.6 \pm 0.8 \mu\text{M}$ and $K_D = 157 \pm 8 \mu\text{M}$, respectively; Sims and Cohen, 2009). Indeed, RAP80 retained its K63-linkage specificity in crosslinking to Ub₂^{PT(8)} (Figure 2C). The orientation of Rap80-tUIM (cyan) in complex with K63-Ub₂ positions Leu8 on the distal Ub unit in close proximity to the UIM of RAP80 (Figure 2D), explaining the efficiency of crosslinking with K63-Ub₂^{PT(8)}. Crosslinking of RAP80^{tUIM} with K48-Ub₂^{PT(8)} was negligible. These results highlight the importance of optimizing the position of the photoleucine residue in Ub^{PT}, depending on targeted receptors. With validation of Ub^{PT} on established Ub receptors, we set out to capture Ub-binding components of protein complexes.

PolyUb^{PT} Identifies Rpn1 as a PolyUb-Binding Protein

Having confirmed that pLeu does not interfere with the hydrophobic nature of recognition by typical Ub-binding proteins and that it can be useful to trap shuttles or stand-alone receptors, we set out to evaluate its specificity in pinpointing Ub-binding proteins within multi-subunit complexes. Proteasomes are made up of some 35 subunits, at least six of which associate with polyUb during the catalytic cycle. Applying our approach to isolate Ub-binding components of a multi-subunit complex specifically (Figure 1E), we found that polyUb^{PT} trapped Rpn10



(legend on next page)

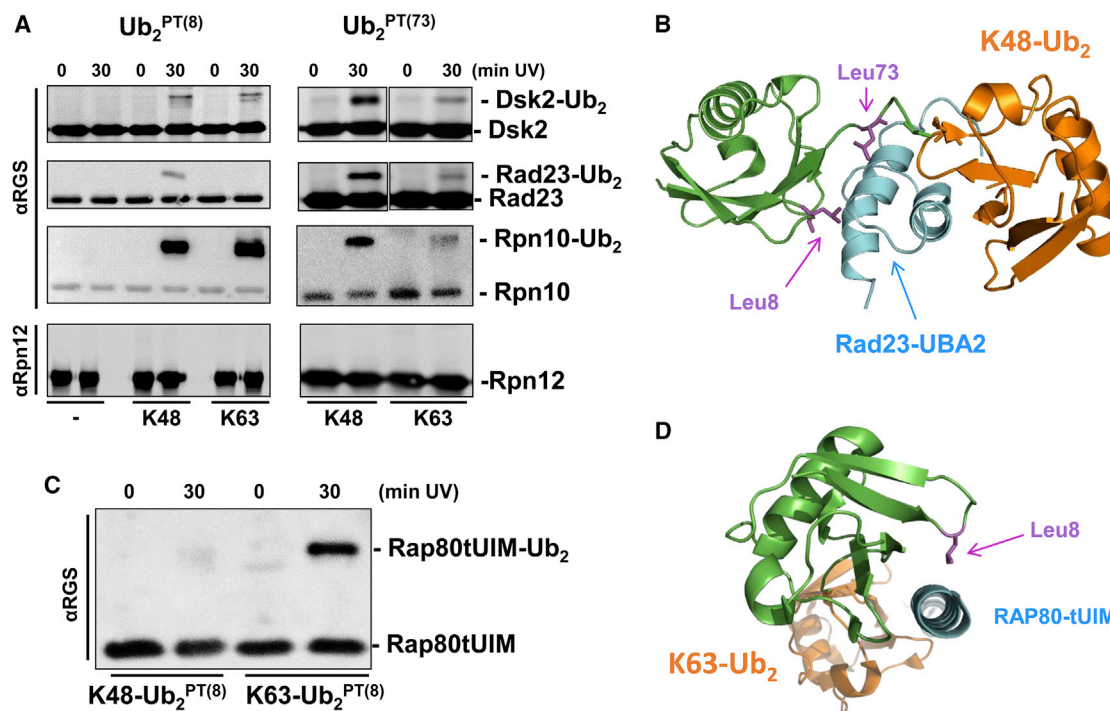


Figure 2. Ub_2^{PT} Crosslink to polyUb-Binding Proteins

(A) K48-linked or K63-linked di Ub^{PT} was crosslinked to Dsk2, Rad23, Rpn10, or a control protein Rpn12 according to the protocol described in Figure 1B. (B) Model of the Rad23-UBA2 molecular structure (cyan) in complex with K48- Ub_2 , distal Ub (green), and proximal Ub (orange) based on PDB: 1ZO6. In this orientation, the proximity of Leu73 and of Leu8 (magenta sticks) of the distal Ub to the receptor are apparent. (C) RAP80-tUIM selectively crosslinks to K63- $\text{Ub}_2^{\text{PT}(8)}$. In this case, RAP80-tUIM efficiently crosslinked to K63- $\text{Ub}_2^{\text{PT}(8)}$ but not to a dimer linked via Lys48, demonstrating that Ub^{PT} allows for trapping of K63-linkage selectivity. (D) Crystal structure of RAP80-tUIM (cyan) in complex with K63- Ub_2 (distal Ub, green; proximal Ub, orange) from PDB: 3A1Q highlights that Leu8 (magenta stick) on the distal Ub is in close proximity to the ligand.

and Rpn1 from intact and functional proteasome complexes, without spuriously crosslinking to neighboring subunits (Figure 3A). Proteasome-bound Rpn10 crosslinked more efficiently to poly $\text{Ub}^{\text{PT}(8)}$, maintaining its properties as a stand-alone protein (Figure 2). In contrast, proteasome-incorporated Rpn1 was trapped more efficiently by K48-poly $\text{Ub}^{\text{PT}(73)}$, suggesting that the orientation by which it binds Ub chains differs from Rpn10 (Figure 3A). It is important to point out that poly Ub^{PT} was specific for polyUb-binding subunits, and despite being in close proximity to other subunits in the same multi-subunit complex, other subunits did not crosslink to poly Ub^{PT} (Figure 3). Interestingly, a proteasome-associated DUB, Ubp6, was trapped by poly Ub^{PT} (Figure S1). Successful crosslinking of Ubp6^{C118A} with poly $\text{Ub}^{\text{PT}(8)}$ highlights the utility of Ub^{PT} to uncover a range of interaction affinities, even transient enzyme-substrate interactions. Together,

these data establish that poly Ub^{PT} can pinpoint subunits that directly associate with Ub within a multi-subunit, multi-tasking complex.

PolyUb chains can anchor at proteasome complexes directly, or may be tethered by auxiliary factors. In order to test the effect of shuttle proteins on crosslinking of poly Ub^{PT} to Ub receptors at proteasome, we incubated purified 26S proteasomes with K48- $\text{Ub}_4^{\text{PT}(73)}$, with or without excess Rad23, to emulate the role of a polyUb-substrate shuttle. We found that the presence of Rad23 had no effect on K48- $\text{Ub}_4^{\text{PT}(73)}$ crosslinking to Rpn1 in the proteasome (Figure 3B). Under these conditions, Rad23 did not alter the ability of Rpn1 to recognize polyUb while retaining its own ability to bind polyUb as evident by crosslinked product with poly Ub^{PT} (Figure 3B). Thus far, poly Ub^{PT} has emerged as a potent tool to accurately and rapidly pinpoint and isolate

Figure 1. Poly Ub^{PT} , a Ubiquitin Variant Containing Photoactivatable Crosslinking Groups

(A) Synthesis of ubiquitin containing photoleucine. Intermediates shown in the diagram with reaction conditions for each step: (i) Fmoc-OSu, 10% aq Na_2CO_3 , tetrahydrofuran, 96%; (ii) solid-phase peptide synthesis; (iii) 95% TFA, 2.5% triisopropylsilane, 2.5% H_2O . (B) Mechanism of photo-crosslinking. After UV irradiation at 355 nm, the diazirine moiety (left) is released as N_2 and forms a highly reactive singlet carbene on the alkyl side chain of Ub (center). The carbene can then react with nearby protein residues or chemical functional groups forming a new covalent bond (right). (C) Enzymatic polymerization of poly Ub^{PT} . Ub^{PT} was polymerized into polyUb chains by incubating with E1, linkage-specific E2 (example shown for K63 chains), and substoichiometric Ub-His₆ (left). Ni^{2+} -NTA separation removed unpolymerized Ub monomers (center). Chains of homogeneous length separated by size exclusion (right). (D) Linkage-specific antibodies recognize di Ub^{PT} in which Leu8 or Leu73 was replaced with photoleucine, similar to cognate diUb. (E) Scheme to detect linkage-specific polyUb-binding subunits using 6xHis tagged poly Ub^{PT} initiated by photoactivation followed by denaturing isolation.

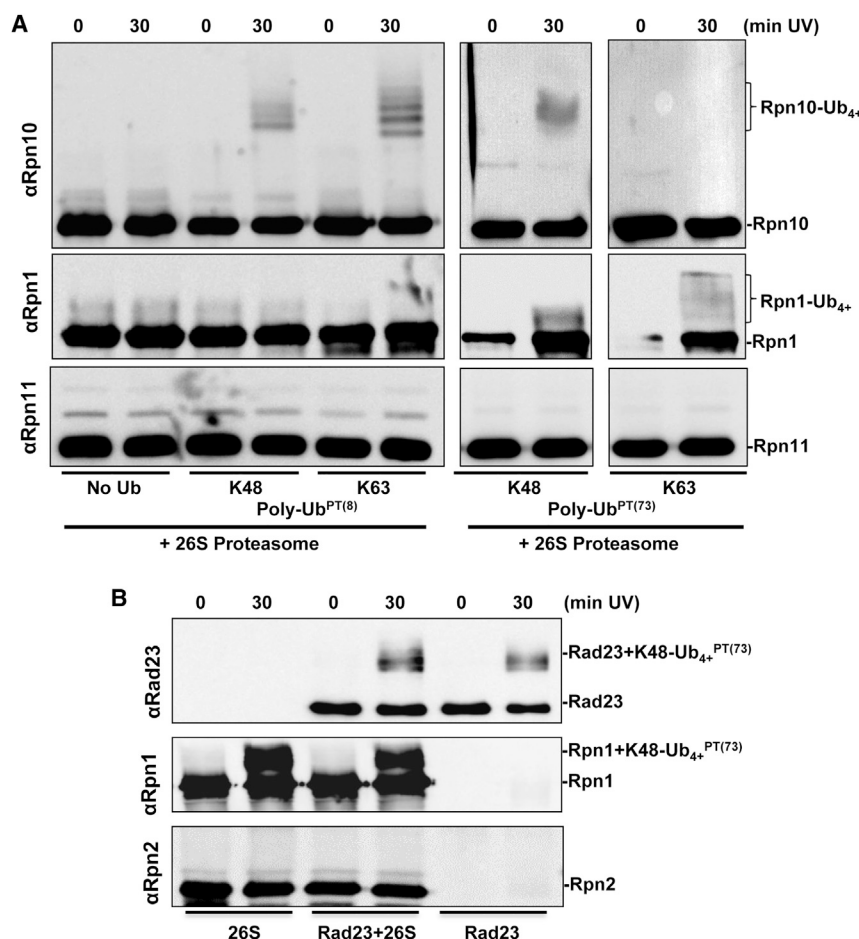


Figure 3. PolyUb^{PT} Crosslinks to Purified Yeast Proteasome

(A) In the proteasome, Rpn10 shows a preference to bind polyUb^{PT(8)} (top panel), while Rpn11 shows no detectable interaction with polyUb^{PT}. (B) K48-Ub₄₊^{PT(73)} retains its ability to crosslink to Rad23 (top panel); Rpn1 retains its ability to recognize polyUb^{PT} in the proteasome regardless of Rad23 (middle panel); no crosslinking is detected with Rpn2 (bottom panel).

product, within 5 min, suggests that the interaction is significant. However, the size and conformational flexibility of Rpn1 posed hurdles for purification strategies and solubility. Therefore, we found that a truncated segment of Rpn1 covering the PC repeats (aa 356–905; Rpn1^{PC}), or even just the first set of PC1 repeats (aa 391–642; Rpn1^{PC1}) were easily purified as soluble monomeric proteins and retained competence to crosslink polyUb^{PT} (Figures 4D, 4E, and S2). Compared with the full-length Rpn1 protein, these smaller polypeptides were more amenable for subsequent biophysical assays such as NMR experiments. K48-linked polyUb^{PT} efficiently trapped Rpn1^{PC}. Once again, the presence of Rad23 had little effect on K48-Ub₄₊^{PT(73)} crosslinking to Rpn1^{PC}, even though Rad23 itself was also competent to bind and crosslink to these K48-linked polyUb

polyUb-binding proteins in mixed or complex environments. With Rpn1 being the newest and least studied of the proteasome-associated polyUb-binding proteins, our focus turned to what additional information polyUb^{PT} can provide on Rpn1 as a potential Ub receptor in the proteasome.

UBL-UBA proteins such as Rad23 constitute the main class of shuttles for polyUb conjugates and dock at the proteasome through their UBL domain to PC repeats situated in the central region of the Rpn1 proteasome subunit. Structurally, Rpn1 can be divided into three segments: a central toroid made up of repetitive alpha-turn-alpha repeats termed PC repeat (Effantin et al., 2009; Kajava, 2002; Lupas et al., 1997), flanked by flexible N and C extensions (Figure 4A). In each PC repeat, the outer α helix contains bulkier amino acid side chains, causing the repetitive structure to curve inward into a concave arc imaged as a closed donut-shaped toroid in proteasomes (Aufderheide et al., 2015; Effantin et al., 2009; Schweitzer et al., 2016). The PC repeats cluster in two, which we term PC1 and PC2 (Figure 4B), interspersed with a highly charged segment for which little structural information is available (Unverdorben et al., 2014). As it happens, UBL (and most likely Ub) binding maps to PC1 (Gomez et al., 2011; Shi et al., 2016). First, we confirmed that polyUb^{PT} was competent to trap full-length recombinant Rpn1 as a stand-alone protein unassociated with 26S complexes (Figure 4C). The relatively fast appearance of crosslinked

chains (Figure 4D). This result may indicate either that multiple sites on Rpn1 associate with Ub or UBLs or that, at stoichiometric ratios, neither ligand binds Rpn1 tightly enough to exclude the other. Nevertheless, association of Rpn1^{PC} with Ub was significant enough that crosslinked products were detected even with unanchored dimeric Ub (K48-Ub₂^{PT(73)}; Figures 4E and S2), indicating that Rpn1 is an inherent Ub binder.

PolyUb-Binding Region of Rpn1

As an integral subunit of the proteasome complex, Rpn1 associates with several neighboring subunits in the 19S. Does this leave sufficient surface area exposed to bind its ligands such as UBLs or polyUb? From current cryo-electron-microscopy-derived proteasome models (PDB: 4CR2), Rpn1 is situated peripherally on the 19S RP touching two AAA ATPase subunits, Rpt1 and Rpt2 (Figure S3). Not surprisingly, most evolutionary conserved residues on the surface of Rpn1 identified with the ConSurf server contacted neighboring subunits Rpt1 and Rpt2 when incorporated into the proteasome, although a few exposed residues that are not in direct contact with any other proteasome subunit are also highly conserved between Rpn1 sequences across eukaryotes (Figure S3). By focusing on Rpn1 (chain Z in PDB: 4CR2) and its two nearest neighbors, it becomes apparent that half of the PC toroid (see previous paragraph) is solvent exposed and suitably positioned to serve as a docking station

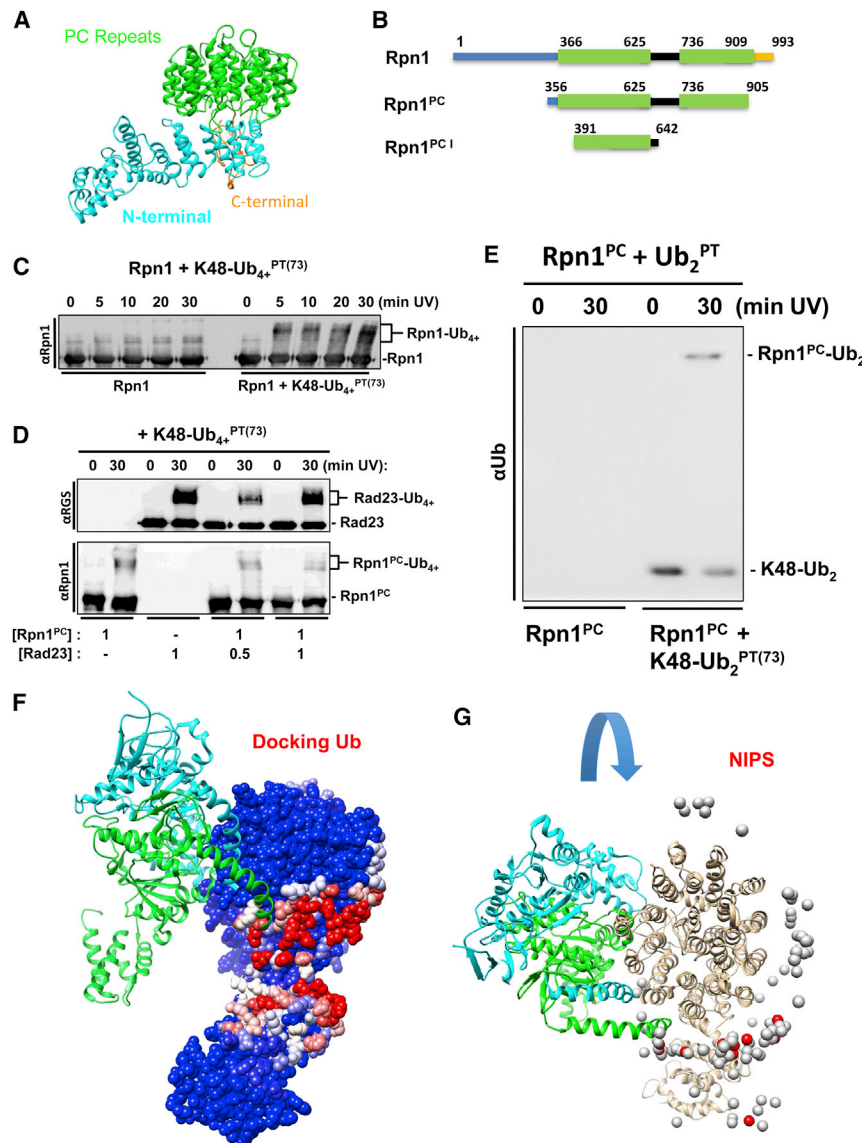


Figure 4. PolyUb^{PT} Crosslinks to First PC Repeat of Rpn1

(A) Rpn1 structure from PDB: 4CR2 (chain Z) with PC repeats (green), N-terminal region (cyan), and flexible linker (gold). (B) Schematic dissection of Rpn1 domains used in the study (PC repeats in green). (C) Time course of crosslinking of K48-Ub₄^{PT(73)} and full-length Rpn1. (D) K48-linked diUb^{PT(73)} was crosslinked to Rpn1^{PC} (Rpn1³⁵⁶⁻⁹⁰⁵). (E) K48-Ub₄^{PT(73)} successfully crosslinks with Rad23 alone and in varying concentrations of Rpn1^{PC} (top). Unexpected crosslinking products of K48-Ub₄^{PT(73)} and Rpn1^{PC} are uncovered with anti-Rpn1 (bottom). (F) Molecular docking analysis using PDB: 4CR2 for the Rpn1 structure and PDB: 1UBQ for ubiquitin. The position of two nearest neighbors in the 19S, Rpt1 and Rpt2, are shown in light blue and green, respectively, according to the EM model. (G) Rpn1 colored by normalized interface propensity values (see STAR Methods; higher values in red) in the context of the proteasome with its interacting subunits: 26S protease regulatory subunit 7 homologs (Rpt1, chain H, colored cyan) and 26S protease regulatory subunit 4 homolog (Rpt6, chain I, colored green). Ub docking does not interfere with binding of RPN1 to the proteasome.

Features of PolyUb Binding to the First PC Region of Rpn1

The PC1 fragment of Rpn1 is small enough to make it amenable for biophysical characterization by NMR assays. Measurements of the ¹⁵N transverse relaxation time (T₂) of backbone amides in monoUb in complex with Rpn1 fragments narrowed the region of association to the PC region, and specifically to the first set of PC repeats, PC1 (Figure 5A, lane I). No binding of polyUb was detected to truncated fragments of Rpn1 that did not contain the

first PC region of Rpn1; we deduced that the first PC region (~aa 356–625) is essential for association of Rpn1 with monoUb through hydrophobic interactions typical of Ub recognition by most receptors (Figure 5A; lanes I, II). The combined results indicate that PC1 is sufficient to bind free Ub (Figure 5A), although we do not rule out that other segments of Rpn1 may participate in binding or in anchoring ligands, as alluded to by the docking experiments (Figures 4F, 4G, and S3). However, merely substituting Leu8 or Ile44 in Ub with alanine diminished its affinity for Rpn1^{PC1}, confirming that the hydrophobic patch on the surface of Ub is central to association with Rpn1 (Figures 5A and S4). Interestingly, using a similar experimental approach, the same PC1 segment could associate with multiple ligands: K48-Ub₂, K63-Ub₂, or the UBL domain of Dsk2 (Figure 5A, lanes III–VI). In order to observe the corresponding changes in Rpn1 upon binding of Ub, we selectively labeled methyl residues of Ile, Leu, Val, and Met in Rpn1^{PC1} with ¹³CH₃ and measured chemical shift perturbations (CSPs) upon titration with increasing concentrations of K48-Ub₂

for substrates or substrate shuttles, possibly explaining the presence of highly conserved exposed residues (Figures 4F and S3). An in silico docking experiment with PyDock WEB server revealed a surface on Rpn1 with low-energy docking poses for complexes with free Ub (Figures 4F, 4G, and S3). The docking experiment was performed on the Rpn1 structure and although interactions were not restricted (e.g., free docking), the most preferred Ub docking sites mapped to the exposed region of the PC domain and to the hinge between the PC domain and the N terminus (red; Figure 4F). When performing docking of Ub onto the PC domain structure (Figure 4G), the 100 most preferred docking results distribute along the exposed edge of the PC ring, particularly along the segment aa ~350–640 that encompasses the highly conserved hydrophobic residues in the first PC repeat (PC1; Figure 4A). This is precisely the area that has been shown before to come in contact with UBL domains of substrate shuttles or with polyUb chains (Shi et al., 2016), encouraging us to utilize Rpn1^{PC1} for further studies.

first PC region of Rpn1; we deduced that the first PC region (~aa 356–625) is essential for association of Rpn1 with monoUb through hydrophobic interactions typical of Ub recognition by most receptors (Figure 5A; lanes I, II). The combined results indicate that PC1 is sufficient to bind free Ub (Figure 5A), although we do not rule out that other segments of Rpn1 may participate in binding or in anchoring ligands, as alluded to by the docking experiments (Figures 4F, 4G, and S3). However, merely substituting Leu8 or Ile44 in Ub with alanine diminished its affinity for Rpn1^{PC1}, confirming that the hydrophobic patch on the surface of Ub is central to association with Rpn1 (Figures 5A and S4). Interestingly, using a similar experimental approach, the same PC1 segment could associate with multiple ligands: K48-Ub₂, K63-Ub₂, or the UBL domain of Dsk2 (Figure 5A, lanes III–VI). In order to observe the corresponding changes in Rpn1 upon binding of Ub, we selectively labeled methyl residues of Ile, Leu, Val, and Met in Rpn1^{PC1} with ¹³CH₃ and measured chemical shift perturbations (CSPs) upon titration with increasing concentrations of K48-Ub₂

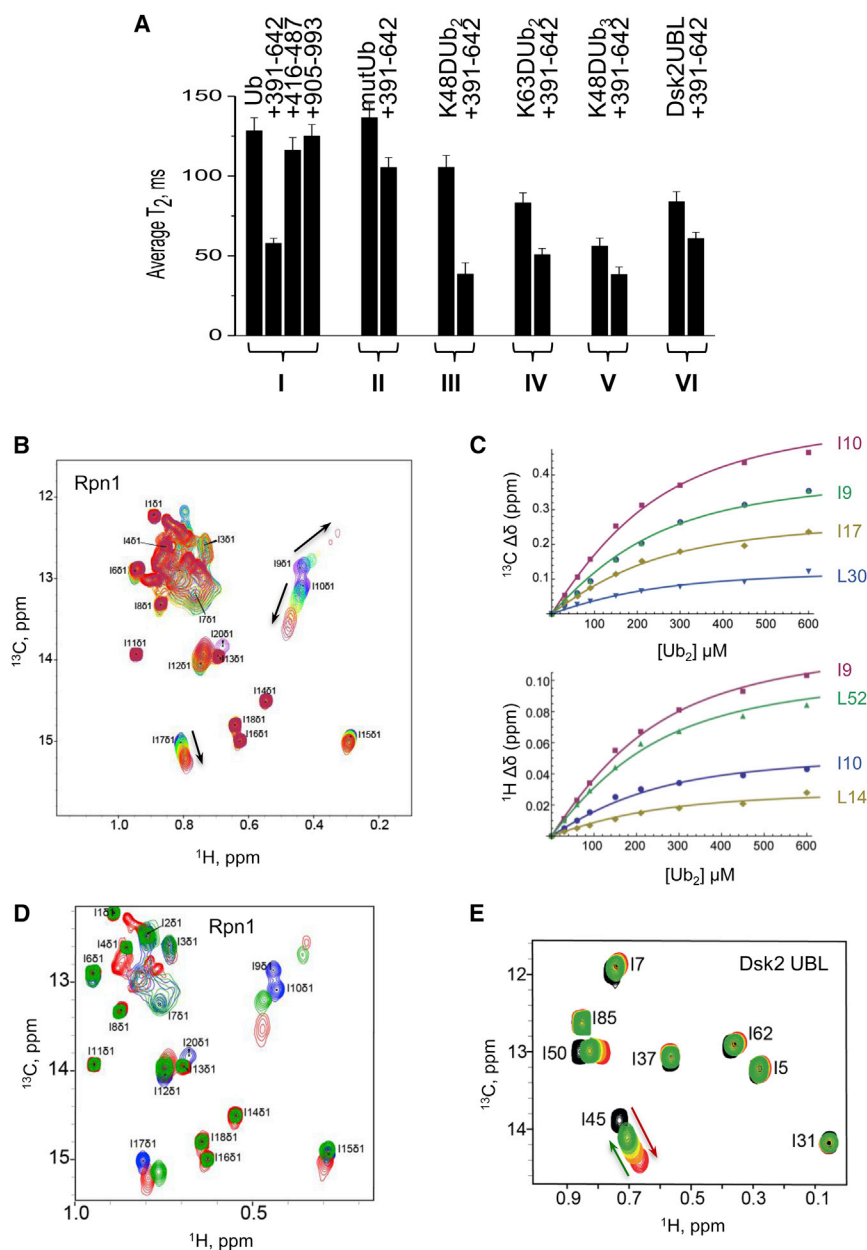


Figure 5. Analysis of the Competition between Ub or Ub₂ and UBL Domains for Binding to Rpn1

(A) ^{15}N T_2 of backbone amides (averaged over secondary structure residues) for the following proteins (left to right): (I) monoUb alone and in the presence of Rpn1^{391–642} or Rpn1^{416–487} or Rpn1^{905–993} at 1:1 molar ratio; (II) Ub mutant (L8A, I44A) alone and in the presence of Rpn1^{391–642} at 1:1 molar ratio; (III) distal Ub of K48-Ub₂ alone and in the presence of Rpn1^{391–642} at 1:1 molar ratio; (IV) distal Ub of K63-Ub₂ alone and in the presence of Rpn1^{391–642} at 1:1 molar ratio; (V) distal Ub of K48-Ub₃ alone and in the presence of Rpn1^{391–642} at 1:1 molar ratio; (VI) Dsk2^{UBL} alone and in the presence of Rpn1^{391–642}.

(B) Overlay of ^1H - ^{13}C heteronuclear multiple-quantum correlation (HMQC) spectra of $^{13}\text{CH}_3$ -ILVM-labeled perdeuterated Rpn1^{391–642} free (purple) and at various points in titration with K48-Ub₂ (from dark blue to red, 3:1 molar ratio). Shown is the spectral region containing CH₃-Ile δ signals; the Rpn1 signals are numbered arbitrarily; the arrows show the directions of signal shifts.

(C) Representative titration curves for select CH₃-Ile δ signals of Rpn1^{391–642} as a function of K48-Ub₂ concentration for ^{13}C (top) and ^1H (bottom) resonances. The solid lines represent the results of a global fit to a 1:1 binding model. The Rpn1 signals are numbered arbitrarily. The average K_D values are summarized in Table 1.

(D) Overlay of ^1H - ^{13}C HMQC spectra of $^{13}\text{CH}_3$ -ILVM-labeled perdeuterated Rpn1^{391–642} in the absence (blue) and presence of K48-Ub₂ (red) or Rad23^{UBL} (green). Shown is the spectral region containing CH₃-Ile δ signals; the Rpn1 signals are numbered arbitrarily. Rpn1 concentration was 250 μM , and Rad23 and K48-Ub₂ were 500 μM each.

(E) Overlay of ^1H - ^{13}C HMQC spectra of $^{13}\text{CH}_3$ -ILVM-labeled perdeuterated Dsk2^{UBL} alone (black), in the presence of ^2H -Rpn1^{391–642} at 2:1 molar ratio (red), and upon subsequent additions of unlabeled K48-Ub₂ up to 16-fold excess (green). At the endpoint of titration, the concentrations are: [Rpn1] = 300 μM , [Dsk2] = 300 μM , [Ub₂] = 4.8 mM. Shown is the spectral region containing CH₃-Ile δ signals; the assignment of Dsk2^{UBL} signals is from Chen et al. (2008). The red and green arrows highlight the signal shifts upon addition of Rpn1^{391–642} and Ub₂, respectively.

(Figure 5B). Titration of $^{13}\text{CH}_3$ -labeled Rpn1^{PC1} (Ile, Leu, Val, and Met residues have a labeled methyl group; $^{13}\text{CH}_3$ -ILVM-Rpn1^{PC1}) with diUb produced a K_D of 112 ± 29 μM (Figure 5C and Table 1), which makes it comparable with or slightly weaker than other polyUb receptors such as Rpn10 (Rosenzweig et al., 2012). Select CSPs of Ile and Leu groups demonstrated that specific hydrophobic residues in the first PC repeat region of Rpn1 participate in binding to Ub and to diUb (Figures 5B and 5C). In addition, these same methyl residues displayed chemical shift changes upon Rpn1 association with Rad23^{UBL} (Figure 5D). A structure of Rad23UBL bound to residues in the same region was observed independently (Chen et al., 2016), confirming that Rpn1^{PC1} likely contains overlapping (or partially overlapping) binding sites for polyUb and for Rad23^{UBL}.

Rpn1^{PC1} bound UBL domains of proteasome shuttles tighter than Ub: Dsk2^{UBL} with $K_D = 22 \pm 12$ μM and Ubp6^{UBL} with $K_D = 40 \pm 31$ μM (Table 1). Titration of Rpn1 with ^{15}N -Rad23^{UBL} caused severe signal broadening in amide signals that precluded accurate determination of signal shifts for K_D determination. The observation of signal broadening indicates intermediate or slow exchange likely due to slow off-rates, compatible with reported tight affinity (Shi et al., 2016). Since signal broadening was not observed for Dsk2 or for diUb at similar conditions, this signifies fundamentally tighter Rpn1 binding to Rad23^{UBL} compared with the other two ligands. Rub1, the UBL protein most closely resembling Ub (Singh et al., 2012), also bound the first PC stretch of Rpn1 with a $K_D = 280 \pm 20$ μM , an affinity comparable with that of monoUb (Table 1). These results indicate that UBL domains of

Table 1. Summary of Rpn1 Interactions

Analyte ^a	Ub (NH)	K48-Ub ₂ (Dist,NH)	Rpn1 (CH3)	K63-Ub ₂ (Dist,NH)	Dsk2 UBL (NH)	Ubp6 UBL (NH)	Rub1 (NH)
Ligand	Rpn1 ^{PC1}	Rpn1 ^{PC1}	K48-Ub ₂	Rpn1 ^{PC1}	Rpn1 ^{PC1}	Rpn1 ^{PC1}	Rpn1 ^{PC1}
K _D (μM)	214 ± 68	116 ± 30	112 ± 29	103 ± 59	22 ± 12	40 ± 31	280 ± 20

^aTitration of Rpn1 to ¹⁵N-Rad23 caused severe signal broadening in amide signals that precluded accurate determination of signal shifts for K_D determination. The observation of signal broadening indicates an intermediate or slow exchange regime, likely due to slow off-rates.

proteasome shuttles have a greater affinity for Rpn1^{PC1} compared with reversible protein modifiers such as polyUb or Rub1 (Table 1).

Having mapped binding of both diUb and UBLs to the first PC region of Rpn1, we wished to evaluate whether they compete for the same site. Although binding of Rad23^{UBL} and Ub have been mapped to same site (Shi et al., 2016), competition assays have not tested their relative affinities, and binding of similar UBLs have not been mapped. We designed a competition experiment to test whether prebound Dsk2^{UBL} is displaced from Rpn1^{PC1} by excess diUb (Figure 5E). Initially, chemical shifts of methyl groups in ¹³CH₃-ILVM-labeled Dsk2^{UBL} were recorded in the free state (i.e., the ligand unbound to a receptor) and in complex with Rpn1^{PC1} (Figure 5E, black to red signals). Titration of this pre-formed complex with increasing concentrations of K48-Ub₂ resulted in partial displacement of Dsk2^{UBL} from Rpn1 at high ratios of diUb to UBL. Comparing the magnitudes of Dsk2^{UBL} signal shifts (average over several residues; Figure 5E) before and after adding K48-Ub₂, we estimate that 33.5% ± 2.4% of Dsk2^{UBL} molecules remain in complex with Rpn1^{PC1} in the presence of 16× concentration of K48-Ub₂. Using a mathematical model for competitive binding of two different ligands to the same site on a protein (Wang, 1995) and taking into account the respective experimental K_D values for Dsk2^{UBL} and for diUb (22 ± 12 μM, 112 ± 29 μM; Table 1), we predicted that the fraction of Rpn1^{PC1}-bound Dsk2^{UBL} should drop from 76.3% ± 5.7% of Dsk2^{UBL} before the addition of diUb to 20.6% ± 10.7% at the endpoint of our titration. Indeed, our experimental results demonstrate a similar behavior to this prediction, with a partial overlap of the respective statistical ranges. The somewhat higher percentage of the Rpn1-bound Dsk2^{UBL} observed in this assay may be the result of errors in the protein concentration measurements, but could also point to another binding site on Rpn1 for Ub₂ molecules. Additional studies will be required to verify this.

The uniqueness of pLeu as a crosslinking reagent is the ability to capture interactions of a hydrophobic nature. Most documented receptors such as Rpn10, Rad23, Dsk2, and Rap80 (Figure 2) recognize Ub via the so-called hydrophobic patch on its surface (centered on Leu8, Ileu44, Val70; Pickart and Fushman, 2004), therefore embedding pLeu into a polyubiquitin chain to generate a Ub^{PT} minimally perturbs hydrophobic residues on its surface, offering the potential to study the “sphere of interactions” revolving around Ub. Having used this approach to pin down association of Ub to the PC stretch of Rpn1 on proteasome complexes (Figures 3 and 4), we turned our attention to the complementary binding surfaces on Ub. Upon titrating ¹⁵N-labeled monoUb with Rpn1^{PC1}, the majority of significant CSPs pointed to hydrophobic residues on the surface of Ub centered on the canonical hydrophobic patch (Figures 6A and

6B). Binding affinities of Rpn1 for K48-linked diUb or for monoUb were derived from a global fit of multiple CSP values upon titrations with ligand and estimated to have a K_D of 116 ± 30 μM or 214 ± 68 μM, respectively (Figures 6C and 6D, Table 1). Even K63-Ub₂ bound Rpn1^{PC1} with a K_D of 103 ± 59 μM (Figure S5), suggesting that Rpn1 can interact with an array of polyUb signals without being particularly discriminatory of linkage type. It is important to clarify that these are apparent affinities that may reflect a variation in interactions between multiple residues on both receptor and ligand. A 2-fold increase in the binding affinity of dimeric over monomeric Ub (K_D dropping from ~215 to ~115 μM) does not imply cooperative binding. Indeed, upon binding of Rpn1, the CSPs from either amide (¹⁵N) or methyl (¹³CH₃-ILVM) groups in either unit of K48-Ub₂ pointed out that L8, I44, and V70 of both proximal and distal Ub units of K48-Ub₂ were perturbed upon binding to Rpn1 (Figures 6E and 6F). These observations suggest that a change in the interface between the two units of Ub occurs from the free to Rpn1-bound K48-Ub₂ (Figure S5).

To summarize, Ub^{PT} is a novel reagent to trap hydrophobic interactions of a variety of polyUb modifications. The first experimental application of polyUb^{PT} pinpointed PC repeats in Rpn1 (Rpn1^{PC1}) as the primary docking site of polyUb on proteasomes. Monitoring reciprocal changes determined that this association is coordinated by hydrophobic residues on the surface of Ub (Figure 6). Beyond Ub recognition, incorporating pLeu into proteins of interest should extend similar possibilities to investigate hydrophobic associations of a plethora of signaling molecules.

DISCUSSION

In this study, we show how polyUb^{PT} can be used effectively to selectively bind, trap, and even isolate the preferred binding partner from a protein mixture, or to pinpoint a receptor on a protein complex containing multiple subunits with diverse properties. By fixing interactions, followed by isolation and identification of co-purifying subunits, crosslinking is a particularly powerful tool to identify the composition of complexes. Crosslinkers can even narrow down recognition elements in each participant. However, transient interactions pose an experimental hurdle for traditional crosslinking approaches. Increasing the reactivity of the functional group in the hope of stabilizing fleeting associations would only amplify the probability of trapping spurious or non-specific interactions during the off time between the main signaling partners. In the current study, we have introduced Ub^{PT} as a general tool for unbiased screening of binding partners of Ub without prior knowledge of the binding partners in order to trap weak transient binders without decreasing specificity, which would render the results uninformative due to false positives.

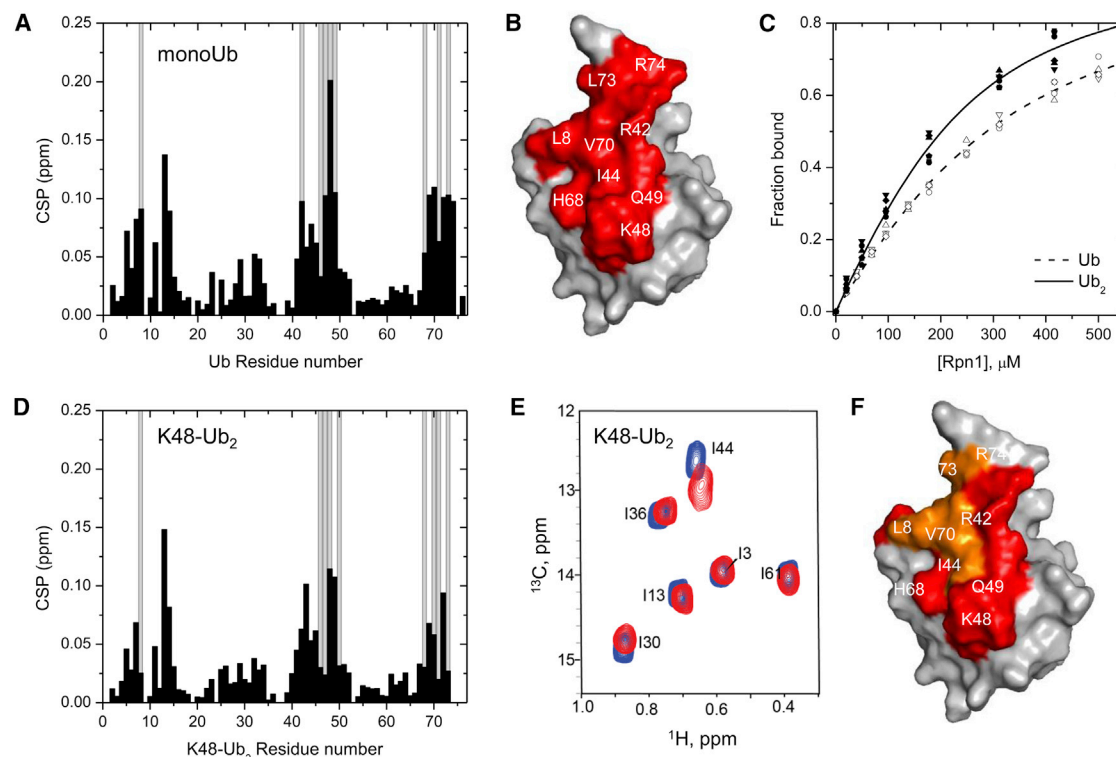


Figure 6. NMR Analysis of the Binding Interactions between Rpn1^{391–642} and MonoUb and DiUb

(A) Amide CSPs (black bars) in monoUb at the endpoint of titration with Rpn1^{PC1} (Rpn1^{391–642}) as a function of residue number. Residues exhibiting strong signal attenuations (>75%) during the titration are marked with gray bars.

(B) Map of the perturbed residues (red, CSP >0.05 ppm and/or signal attenuations) on the surface of Ub. Some residues are indicated.

(C) Titration curves for several residues in monoUb (open symbols) or K48-Ub₂ (solid symbols) as a function of Rpn1 concentration. The lines (dashed or solid, respectively) represent the results of a global fit of multiple CSP values upon titrations with ligand to a 1:1 binding model. The titrations started with 200 μM Ub or Ub₂, and went up to 4.1-fold molar excess of Rpn1^{PC1} for monoUb and 3.1 for Ub₂. Binding affinities of Rpn1 for monoUb or for K48-linked diUb were derived from a global fit (residues 7, 13, 14, 70, 72 in monoUb; 14, 44, 45, 49, 69 in diUb) and estimated to have a K_D of 214 ± 68 and 116 ± 30 μM, respectively, which was identical within experimental error to the K_D of 112 ± 29 μM obtained from the reciprocal titration of ¹³CH₃-ILVM-Rpn1^{PC1} with unlabeled K48-Ub₂ (summarized in Table 1).

(D) Amide CSPs (black bars) in the distal Ub of K48-Ub₂ at the endpoint of titration with Rpn1^{PC1} as a function of residue number. Residues showing strong signal attenuations (>75%) during the titration are marked with gray bars. Note that the residues exhibiting perturbations in K48-Ub₂ are essentially the same as in monoUb (A and B). Similar residues in K63-Ub₂ showed perturbations upon titration with Rpn1^{PC1} (Figure S5).

(E) Overlay of ¹H-¹³C HMQC spectra of ¹³CH₃-labeled ILVM residues in perdeuterated K48-Ub₂ in the absence (blue) or presence (red) of perdeuterated Rpn1^{PC1}. Only methyl groups of Ile, Leu, Val, and Met were selectively ¹³CH₃-labeled in an otherwise deuterated background (²H, ¹³CH₃-ILVM). Strong CSPs were recorded primarily in L8, I44, and V70 of both proximal and distal Ub units. Shown is the spectral region containing CH₃-Ile δ signals.

(F) Residues on Ub that exhibited spectral perturbations upon addition of Rpn1 to K48-Ub₂; amide data are colored red and on top of them methyl data are colored orange.

Design of modifications on side chains amenable for cross-linking (or of fluorescent or paramagnetic tags for other biophysical techniques) to map protein-protein interactions often requires knowledge of protein sequence and structure to obtain successful results. Chemical crosslinkers traditionally link between neighboring amine or thiol groups, which can be either in *cis* on a single protein or in *trans* between binding partners. This property may pose a hurdle for traditional crosslinkers to capture Ub-binding proteins as recognition of Ub often utilizes hydrophobic interactions. At the same time, the Ub molecule is naturally suited for integration of photoleucine given that hydrophobic residues partake in interactions with Ub-interacting proteins such as receptors, DUBs, or conjugating enzymes. Specifically, two key leucine residues on Ub, Leu8 and Leu73, are solvent exposed and are known to participate in binding

associations. Integration of photoleucine into Ub allowed for a highly reactive crosslinking agent that could react with protein backbones in close proximity, yet facetly quenched by solvent to limit spurious interactions (Figure 1). Following photoactivation, the reactive singlet carbene on the alkyl side chain of pLeu can bond covalently with a number of common functional groups in proteins, guaranteeing that efficient crosslinking is not restricted to precise positioning of a limited set of residues (e.g., lysine, cysteine) thereby increasing the likelihood of trapping binding partners. However, as hydroxyl groups are also prevalent in aqueous environments, the effective chemical half-life of the reactive singlet carbene on unattached “Trap” is short; the trap is essentially self-limiting due to quenching by water. This property decreases crosslinking to spurious non-specific proteins ensuring that pLeu is specific for meaningful nearest

neighbors, even of transient associations. As we demonstrated, the reaction was rapid with detectable product within 5 min. The added benefit of a photoactivatable group gives Ub^{PT} users complete control over when to initiate the crosslinking reaction. Importantly, Ub^{PT} is a modular reagent that is easily incorporated into polyUb^{PT} and can be used to differentiate between linkage-specific UBDs.

Crosslinking approaches have been successful for determining proteasome architecture (Bohn et al., 2010; Forster et al., 2009; Hartmann-Petersen et al., 2001; Lasker et al., 2012; Sharon et al., 2006), however they were not successful in detecting transient interactions of proteasome-interacting-proteins. Our polyUb-based photo-crosslinking reagents, which we term polyUb^{PT}, were successfully applied to 26S proteasome complexes, subunits, and associated receptors. Rpn1 emerged as the highest capacity Ub-binding subunit of the proteasome, able to form a complex with polyUb and UBL domains. By docking shuttles and associating with Ub, Rpn1 may aid unloading of ubiquitinated cargo onto the proteasome for further treatment (Figure S6). While this study was under preparation, the capacity of Rpn1 to associate with Ub was substantiated independently (Shi et al., 2016). Using a combination of techniques, the authors elegantly demonstrated that Rpn1 harbors two binding sites: T1 for UBL domains and for Ub, and T2 for the UBL domain of Ubp6. The specific residues on the T1 site that bind Ub were identified by solving an NMR structure of a segment of Rpn1 associated to Ub or diUb. This site falls into the first PC repeat of Rpn1, the same region that was found sufficient to be captured by polyUb^{PT}. Moreover, PolyUb^{PT} was able to pinpoint and isolate Rpn1 out of the intact 26S proteasome complex, demonstrating that association with Ub is retained in both free and proteasome-incorporated forms. The same residues also associate with Rad23 and can be competed out by excess Dsk2UBL, hinting at possible unloading of ubiquitinated cargo from shuttle proteins to proteasome.

Rpn1 is the first Ub-binding protein associated with the proteasome complex that is encoded by an essential gene in *S. cerevisiae*. Typically, proteasome-associated polyUb-binding proteins have been classified into two categories: (1) delivery proteins or shuttles, whose association with the proteasome is transient in nature (e.g., Rad23/hHR23, Dsk2/hPLIC/Ubiquilin, Ddi1/DDI1) and (2) bona fide receptors (Rpn10/S5a, Rpn13/ADRM-1). Yet, in *S. cerevisiae*, none of the Ub-associating proteins are strictly essential (Finley et al., 2012). Two additional proteasome subunits interact with polyUb, the DUB Ubp6/USP14 (Aufderheide et al., 2015; Mansour et al., 2015; Peth et al., 2009) and an ancillary tethering component Sem1/Dss1 (Paraskevopoulos et al., 2014), yet they are also non-essential. On a tangential note, the metalloprotease Rpn11/PSMD14 (Aufderheide et al., 2015; Luan et al., 2016; Mansour et al., 2015; Pathare et al., 2014) and the ATPase Rpt5 (Lam et al., 2002) have also been suggested to interact with polyUb in some capacity and are essential subunits, yet their contribution to recruitment or anchoring of polyUb at proteasome complexes has not been defined. Thus far, the prevailing view has been that these subunits work in parallel as redundant receptors and no single Ub-binding subunit serves as the primary docking site on the proteasome. This view is being revised, now that independent studies have demonstrated the propensity of Rpn1 to associate with polyUb at the proteasome.

Through its sheer size (being the largest subunit in the 26S proteasome complex) and its structural features, Rpn1 is naturally set up to scaffold several adjacent subunits and provide a docking site for proteasome-associating factors (Effantin et al., 2009; He et al., 2012; Rosenzweig et al., 2012). Light-induced crosslinking with engineered Ub^{PT} narrowed down polyUb binding to the first PC region of Rpn1, overlapping with binding sites reported for UBL domains such as those found in proteasome shuttles (Elsasser et al., 2002; Gomez et al., 2011; Rosenzweig et al., 2012; Yun et al., 2013). Yet the functional relationship of Rpn1 to other polyUb-binding components on the proteasome is unclear, given the convoluted network of interactions of polyUb and UBLs (at comparable affinities) to multiple receptors at the proteasome (Kang et al., 2006, 2007; Matihuhin et al., 2008; Mueller and Feigon, 2003; Mueller et al., 2004; Zhang et al., 2009a, 2008, 2009b). While Rpn1 is capable of directly binding both K48- and K63-linked polyUb, its affinity for the UBL domain of the UBL-UBA family of shuttles is tighter than for unanchored chains. It is, therefore, likely that shuttles direct and aid targeting of polyUb conjugates to Rpn1. In this manner, a single proteasomal subunit, Rpn1, coordinates docking of substrate shuttles, unloading of substrates, and anchoring of polyUb conjugates, defining the first mechanistic step of proteasome action.

PolyUb is a complex signal made up of repeating units that are assembled in an almost endless number of possible configurations (Nakasone et al., 2013). In order to achieve the desired outcome, each configuration of polyUb should be recognized precisely, deciphered, and conveyed to the proper pathway. To this end, a multitude of proteins discriminate among the plethora of polyUb signals by means of embedded UBDs. Consequently, most interactions with Ub are transient, with intermediate complexes serving to shuttle polyUb conjugates as cargo while also protecting the signal from disassembly by DUBs (Hartmann-Petersen et al., 2003; Wilkinson et al., 2001). Moderate affinities (tens to hundreds of μ M) for polyUb chains (Fushman and Wilkinson, 2011; Winget and Mayor, 2011) often reflect high off-rates from shuttles and hence the transient nature of many polyUb signals. Even at a destination such as the proteasome, recruitment and anchoring of polyUb is just the beginning of a multi-step trajectory. As a substrate unfolds and is translocated into the 20S CP, the polyUb signal is relayed between receptors and finally handed over to proteasome-associated DUBs for release (Aufderheide et al., 2015; Bhattacharyya et al., 2014; Matyskiela et al., 2013; Peth et al., 2013b; Sledz et al., 2013a; Sledz et al., 2013b; Unverdorben et al., 2014). Although many proteins with affinity for Ub or polyUb have been uncovered through a variety of experimental approaches (Fushman and Wilkinson, 2011; Husnjak and Dikic, 2012; Scott et al., 2015; Winget and Mayor, 2011), the transient nature of association and fast exchange rates pose a hurdle to full mapping of the associated Ub-interactome. The novel set of phototrap reagents based on the Ub polymer proved powerful in exposing new insight on Ub-binding entities.

PolyUb^{PT}, as its name implies, was able to trap a specific transient interaction in a multi-subunit, multi-catalytic, molecular machine. This study lays the foundation for the future use of polyUb^{PT} to discover interactions of Ub in new systems and beyond to unrelated proteins. The lability of light-induced photo-leucine as a crosslinking reagent, combined with the flexibility of

enzymatic polymerization of Ub^{PT} enables low-resolution surface mapping of receptor-ligand interfaces. PolyUb^{PT} demonstrates that different UBDs such as the newly exposed PC repeat stretch in Rpn1, UIMs, or UBA domains, contact different elements in the Ub ligand. The specificity of Ub chain recognition is not limited to the linkage or to residues directly surrounding the isopeptide linkage but involves additional residues. Hence, the UIM of RAP80 meets different surface areas on the Ub chain than the UIM of Rpn10. The properties of polyUb^{PT} should allow characterization of interactions with intermediate binding affinities and even for unambiguous detection of elusive polyUb-binding proteins. With Ub^{PT} validated on a diverse set of established Ub receptors, Ub^{PT} emerges as a powerful tool to chart the plethora of Ub-associating proteins found in the Ub signaling system. From a qualitative point of view, the broad incorporation of Ub^{PT} into diverse polyUb chains highlights the non-invasive nature of the photoleucine probe on Ub chain synthesis and, most importantly, without altering the hydrophobic nature on which many of its partners rely for proper recognition. We conclude that Ub^{PT} is a modular reagent that provides advantages over conventional crosslinking reagents for studying Ub-associating proteins in extract, in complex, or in isolation.

SIGNIFICANCE

How shuttles, receptors, and multiple binding subunits on the proteasome relay the polyUb signal between them has not been deciphered. Through the application of novel UV light-inducible crosslinking agents, Ub^{PT} and Ub^{PT}-spiked polyUb chains, we were successful in capturing proteasome-associated Ub-binding subunits. The embedded photoleucine crosslinker minimally interfered with recognition of Ub moieties and thus enabled characterization of polyUb association with an essential proteasome subunit, Rpn1. A hydrophobic patch centered on L8, I44, and V70 on the surface of Ub tethers to hydrophobic residues on the exposed surface of proteasome-incorporated Rpn1. Rpn1 binds Ub chains polymerized through either K48 or K63 linkages, and retains its Ub-binding properties as a free stand-alone protein. The flexible α -helical PC repeat sequence on Rpn1 is sufficiently broad to anchor polyUb and UBL-containing proteins simultaneously. This provides insight on how the polyUb signal is transferred from shuttles to receptors and expands our knowledge of Ub-binding subunits at the proteasome. Hybrid synthesis (i.e., chemical and enzymatic) of polyUb chains of well-defined linkage, combined with the site of the photoactivatable crosslinker, is highly adaptable for covalently trapping hydrophobic interactions in diverse systems beyond the Ub system. To conclude, Ub^{PT} is a modular reagent that provides advantages over conventional crosslinking reagents for studying Ub-associating proteins in complex or in isolation.

STAR★METHODS

Detailed methods are provided in the online version of this paper and include the following:

● KEY RESOURCES TABLE

- **CONTACT FOR REAGENT AND RESOURCE SHARING**
- **EXPERIMENTAL MODEL AND SUBJECT DETAILS**
- **METHOD DETAILS**
 - Plasmid Construction and Protein Purification
 - Purification of Rpn1 and Rpn1 Fragments
 - Methyl Labelling Rpn1^{PC1}
 - Assembly of K48- and K63-Linked polyUb^{PT(8)} and polyUb^{PT(73)} Chains
 - Yeast Proteasome Purification
 - Western Blot Analysis
 - Assembly of Ub₂ Chains for NMR Measurements
 - NMR Measurements
 - Ub^{PT} Crosslinking Conditions
 - Docking Simulations and Bioinformatics Analysis
 - Chemical Methods Synthesis of Monomeric Ub^{PT(8)} and Ub^{PT(73)}
 - Compound Synthesis and Characterization
 - Solid Phase Peptide Synthesis of Ub Containing Photoleucine
 - HPLC Purification of Ub Containing Photoleucine
 - Analysis of Purified Ubiquitin Incorporated with Photoleucine
 - LC-MS Analysis of the Purified Ubiquitin Containing Photo-Leucine

SUPPLEMENTAL INFORMATION

Supplemental Information includes six figures and ten schemes and can be found with this article online at <http://dx.doi.org/10.1016/j.chembiol.2017.02.013>.

AUTHOR CONTRIBUTIONS

F.E.O. devised the UbPT design. D.S.H. and F.E.O. carried out the synthesis of UbPT monomers. W.M. and M.C. constructed the plasmids for Rpn1 fragments and performed the crosslinking experiments. W.M., M.C., and M.A.N. isolated recombinant proteins and carried out hybrid synthesis of polyUb^{PT}. Z.Y. purified 26S proteasome and aided in proteasome-based crosslinking experiments. R.R. and L.E.K. isolated methyl-labeled Rpn1^{PC1} and carried out methyl-TROSY-based experiments. ¹⁵N experiments were designed and carried out by R.S. and D.F. Docking simulations and bioinformatics analysis was managed by F.G. L.E.K., D.F., H.O., and M.H.G. funded the project and coordinated the cooperation and experimental design. All authors contributed to writing the final version of the manuscript.

ACKNOWLEDGMENTS

We thank Dris El Atmioui for peptide synthesis. We thank Carlos A. Castañeda for help with the synthesis of isotopically labeled diUb. Noa Reis is acknowledged for help with the cloning design and construction of plasmids and general advice. W.M. is supported in part by an ISF council for Higher Education Outstanding Minority (VATAT) fellowship, M.C. is supported through the EU Seventh Framework Programme (FP7A-PEOPLE-2011-ITN), M.A.N. is supported by a Fulbright postdoctoral fellowship and the Aly Kaufman Fellowship Trust at the Technion. This work was supported in part by a grant from the Netherlands Foundation for Scientific Research (NWO) to H.O. and a grant from the Canadian Institutes of Health Research and the Natural Sciences and Engineering Research Council of Canada (to L.E.K.) and by NIH grants GM065334 and R21NS093454 (to D.F.) and GM095755 (to D.F. and M.H.G.), a USA-Israel Binational Science Foundation grant (to D.F. and M.H.G.), and an Israel Science Foundation grant 909-14 to M.H.G. H.O. and F.E.O. declare competing financial interests as co-founder and shareholder of UbiQ Bio BV.

Received: May 9, 2016
Revised: December 29, 2016
Accepted: February 23, 2017
Published: March 16, 2017

REFERENCES

- Aufderheide, A., Beck, F., Stengel, F., Hartwig, M., Schweitzer, A., Pfeifer, G., Goldberg, A.L., Sakata, E., Baumeister, W., and Forster, F. (2015). Structural characterization of the interaction of Ubp6 with the 26S proteasome. *Proc. Natl. Acad. Sci. USA* **112**, 8626–8631.
- Bashore, C., Dambacher, C.M., Goodall, E.A., Matyskiela, M.E., Lander, G.C., and Martin, A. (2015). Ubp6 deubiquitinase controls conformational dynamics and substrate degradation of the 26S proteasome. *Nat. Struct. Mol. Biol.* **22**, 712–719.
- Beckwith, R., Estrin, E., Worden, E.J., and Martin, A. (2013). Reconstitution of the 26S proteasome reveals functional asymmetries in its AAA+ unfoldase. *Nat. Struct. Mol. Biol.* **20**, 1164–1172.
- Bhattacharyya, S., Yu, H., Mim, C., and Matouschek, A. (2014). Regulated protein turnover: snapshots of the proteasome in action. *Nat. Rev. Mol. Cell Biol.* **15**, 122–133.
- Bohn, S., Beck, F., Sakata, E., Walzthoeni, T., Beck, M., Aebersold, R., Forster, F., Baumeister, W., and Nickell, S. (2010). Structure of the 26S proteasome from *Schizosaccharomyces pombe* at subnanometer resolution. *Proc. Natl. Acad. Sci. USA* **107**, 20992–20997.
- Castaneda, C.A., Kashyap, T.R., Nakasone, M.A., Krueger, S., and Fushman, D. (2013). Unique structural, dynamical, and functional properties of k11-linked polyubiquitin chains. *Structure* **21**, 1168–1181.
- Chen, T., Zhang, D., Matihun, Y., Glickman, M., and Fushman, D. (2008). ¹H, ¹³C, and ¹⁵N resonance assignment of the ubiquitin-like domain from Dsk2p. *Biomol. NMR Assign.* **2**, 147–149.
- Chen, X., Randles, L., Shi, K., Tarasov, S.G., Aihara, H., and Walters, K.J. (2016). Structures of Rpn1 T1:Rad23 and hRpn13:hPLIC2 reveal distinct binding mechanisms between substrate receptors and shuttle factors of the proteasome. *Structure* **24**, 1257–1270.
- Cheng, T.M., Blundell, T.L., and Fernandez-Recio, J. (2007). pyDock: electrostatics and desolvation for effective scoring of rigid-body protein-protein docking. *Proteins* **68**, 503–515.
- Diaz-Martinez, L.A., Kang, Y., Walters, K.J., and Clarke, D.J. (2006). Yeast UBL-UBA proteins have partially redundant functions in cell cycle control. *Cell Div.* **1**, 28.
- Effantin, G., Rosenzweig, R., Glickman, M.H., and Steven, A.C. (2009). Electron microscopic evidence in support of alpha-solenoid models of proteasomal subunits Rpn1 and Rpn2. *J. Mol. Biol.* **386**, 1204–1211.
- El Oualid, F., Merx, R., Ekkebus, R., Hameed, D.S., Smit, J.J., de Jong, A., Hilkmann, H., Sixma, T.K., and Ovaa, H. (2010). Chemical synthesis of ubiquitin, ubiquitin-based probes, and diubiquitin. *Angew. Chem. Int. Ed.* **49**, 10149–10153.
- Elsasser, S., Gali, R.R., Schwickart, M., Larsen, C.N., Leggett, D.S., Muller, B., Feng, M.T., Tubing, F., Dittmar, G.A., and Finley, D. (2002). Proteasome subunit Rpn1 binds ubiquitin-like protein domains. *Nat. Cell Biol.* **4**, 725–730.
- Elsasser, S., Chandler-Militello, D., Muller, B., Hanna, J., and Finley, D. (2004). Rad23 and Rpn10 serve as alternative ubiquitin receptors for the proteasome. *J. Biol. Chem.* **279**, 26817–26822.
- Fatimababy, A.S., Lin, Y.L., Usharani, R., Radjacommar, R., Wang, H.T., Tsai, H.L., Lee, Y., and Fu, H. (2010). Cross-species divergence of the major recognition pathways of ubiquitylated substrates for ubiquitin/26S proteasome-mediated proteolysis. *FEBS J.* **277**, 796–816.
- Finley, D. (2009). Recognition and processing of ubiquitin-protein conjugates by the proteasome. *Annu. Rev. Biochem.* **78**, 477–513.
- Finley, D., Ulrich, H.D., Sommer, T., and Kaiser, P. (2012). The ubiquitin-proteasome system of *Saccharomyces cerevisiae*. *Genetics* **192**, 319–360.
- Forster, F., Lasker, K., Beck, F., Nickell, S., Sali, A., and Baumeister, W. (2009). An atomic model AAA-ATPase/20S core particle sub-complex of the 26S proteasome. *Biochem. Biophys. Res. Commun.* **388**, 228–233.
- Fushman, D., and Wilkinson, K.D. (2011). Structure and recognition of polyubiquitin chains of different lengths and linkage. *F1000 Biol. Rep.* **3**, 26.
- Gabb, H.A., Jackson, R.M., and Sternberg, M.J. (1997). Modelling protein docking using shape complementarity, electrostatics and biochemical information. *J. Mol. Biol.* **272**, 106–120.
- Girod, P.A., Fu, H.Y., Zryd, J.P., and Vierstra, R.D. (1999). Multiubiquitin chain binding subunit MCB1 (RPN10) of the 26S proteasome is essential for developmental progression in *Physcomitrella patens*. *Plant Cell* **11**, 1457–1471.
- Glaser, F., Pupko, T., Paz, I., Bell, R.E., Bechor-Shental, D., Martz, E., and Ben-Tal, N. (2003). ConSurf: identification of functional regions in proteins by surface-mapping of phylogenetic information. *Bioinformatics* **19**, 163–164.
- Glickman, M.H., and Adir, N. (2004). The proteasome and the delicate balance between destruction and rescue. *PLoS Biol.* **2**, E13.
- Glickman, M.H., and Ciechanover, A. (2002). The ubiquitin-proteasome proteolytic pathway: destruction for the sake of construction. *Physiol. Rev.* **82**, 373–428.
- Glickman, M., and Coux, O. (2001). Purification and characterization of proteasomes from *Saccharomyces cerevisiae*. *Curr. Protoc. Protein Sci. Chapter 21*. Unit 21 25.
- Gomez, T.A., Kolawa, N., Gee, M., Sweredoski, M.J., and Deshaies, R.J. (2011). Identification of a functional docking site in the Rpn1 LRR domain for the UBA-UBL domain protein Ddi1. *BMC Biol.* **9**, 33.
- Grosdidier, S., Pons, C., Solernou, A., and Fernandez-Recio, J. (2007). Prediction and scoring of docking poses with pyDock. *Proteins* **69**, 852–858.
- Guterman, A., and Glickman, M.H. (2004). Deubiquitinating enzymes are IN/ (trinsic to proteasome function). *Curr. Protein Pept. Sci.* **5**, 201–211.
- Hall, J.B., and Fushman, D. (2003). Characterization of the overall and local dynamics of a protein with intermediate rotational anisotropy: differentiating between conformational exchange and anisotropic diffusion in the B3 domain of protein G. *J. Biomol. NMR* **27**, 261–275.
- Hamazaki, J., Iemura, S., Natsume, T., Yashiroda, H., Tanaka, K., and Murata, S. (2006). A novel proteasome interacting protein recruits the deubiquitinating enzyme UCH37 to 26S proteasomes. *EMBO J.* **25**, 4524–4536.
- Hamazaki, J., Hirayama, S., and Murata, S. (2015). Redundant roles of Rpn10 and Rpn13 in recognition of ubiquitinated proteins and cellular homeostasis. *PLoS Genet.* **11**, e1005401.
- Hartmann-Petersen, R., Tanaka, K., and Hendil, K.B. (2001). Quaternary structure of the ATPase complex of human 26S proteasomes determined by chemical cross-linking. *Arch. Biochem. Biophys.* **386**, 89–94.
- Hartmann-Petersen, R., Hendil, K.B., and Gordon, C. (2003). Ubiquitin binding proteins protect ubiquitin conjugates from disassembly. *FEBS Lett.* **535**, 77–81.
- He, J., Kulkarni, K., da Fonseca, P.C., Krutauz, D., Glickman, M.H., Barford, D., and Morris, E.P. (2012). The structure of the 26S proteasome subunit Rpn2 reveals its PC repeat domain as a closed toroid of two concentric alpha-helical rings. *Structure* **20**, 513–521.
- Hershko, A., and Ciechanover, A. (1998). The ubiquitin system. *Annu. Rev. Biochem.* **67**, 425–479.
- Hofmann, K. (2009). Ubiquitin-binding domains and their role in the DNA damage response. *DNA Repair (Amst)* **8**, 544–556.
- Hofmann, K., and Bucher, P. (1996). The UBA domain: a sequence motif present in multiple enzyme classes of the ubiquitination pathway. *Trends Biochem. Sci.* **21**, 172–173.
- Hurley, J.H., Lee, S., and Prag, G. (2006). Ubiquitin-binding domains. *Biochem. J.* **399**, 361–372.
- Husnjak, K., and Dikic, I. (2012). Ubiquitin-binding proteins: decoders of ubiquitin-mediated cellular functions. *Annu. Rev. Biochem.* **81**, 291–322.
- Husnjak, K., Elsasser, S., Zhang, N., Chen, X., Randles, L., Shi, Y., Hofmann, K., Walters, K.J., Finley, D., and Dikic, I. (2008). Proteasome subunit Rpn13 is a novel ubiquitin receptor. *Nature* **453**, 481–488.

- Janz, J.M., Ren, Y., Looby, R., Kazmi, M.A., Sachdev, P., Grunbeck, A., Haggis, L., Chinnapen, D., Lin, A.Y., Seibert, C., et al. (2011). Direct interaction between an allosteric agonist pepducin and the chemokine receptor CXCR4. *J. Am. Chem. Soc.* **133**, 15878–15881.
- Jimenez-Garcia, B., Pons, C., and Fernandez-Recio, J. (2013). pyDockWEB: a web server for rigid-body protein-protein docking using electrostatics and desolvation scoring. *Bioinformatics* **29**, 1698–1699.
- Kajava, A.V. (2002). What curves alpha-solenoids? Evidence for an alpha-helical toroid structure of Rpn1 and Rpn2 proteins of the 26 S proteasome. *J. Biol. Chem.* **277**, 49791–49798.
- Kang, Y., Vossler, R.A., Diaz-Martinez, L.A., Winter, N.S., Clarke, D.J., and Walters, K.J. (2006). UBL/UBA ubiquitin receptor proteins bind a common tetra-ubiquitin chain. *J. Mol. Biol.* **356**, 1027–1035.
- Kang, Y., Chen, X., Lary, J.W., Cole, J.L., and Walters, K.J. (2007). Defining how ubiquitin receptors hHR23a and S5a bind polyubiquitin. *J. Mol. Biol.* **369**, 168–176.
- Kim, I., Mi, K., and Rao, H. (2004). Multiple interactions of rad23 suggest a mechanism for ubiquitylated substrate delivery important in proteolysis. *Mol. Biol. Cell* **15**, 3357–3365.
- Lam, Y.A., Lawson, T.G., Velayutham, M., Zweier, J.L., and Pickart, C.M. (2002). A proteasomal ATPase subunit recognizes the polyubiquitin degradation signal. *Nature* **416**, 763–767.
- Lander, G.C., Estrin, E., Matyskiela, M.E., Bashore, C., Nogales, E., and Martin, A. (2012). Complete subunit architecture of the proteasome regulatory particle. *Nature* **482**, 186–191.
- Lasker, K., Forster, F., Bohn, S., Walzthoeni, T., Villa, E., Unverdorben, P., Beck, F., Aebersold, R., Sali, A., and Baumeister, W. (2012). Molecular architecture of the 26S proteasome holocomplex determined by an integrative approach. *Proc. Natl. Acad. Sci. USA* **109**, 1380–1387.
- Lee, M.J., Lee, B.H., Hanna, J., King, R.W., and Finley, D. (2011). Trimming of ubiquitin chains by proteasome-associated deubiquitinating enzymes. *Mol. Cell Proteomics* **10**, R110 003871.
- Lowe, E.D., Hasan, N., Trempe, J.F., Fonso, L., Noble, M.E., Endicott, J.A., Johnson, L.N., and Brown, N.R. (2006). Structures of the Dsk2 UBL and UBA domains and their complex. *Acta Crystallogr. D Biol. Crystallogr.* **62**, 177–188.
- Lu, Y., Lee, B.H., King, R.W., Finley, D., and Kirschner, M.W. (2015). Substrate degradation by the proteasome: a single-molecule kinetic analysis. *Science* **348**, 1250834.
- Luan, B., Huang, X., Wu, J., Mei, Z., Wang, Y., Xue, X., Yan, C., Wang, J., Finley, D.J., Shi, Y., et al. (2016). Structure of an endogenous yeast 26S proteasome reveals two major conformational states. *Proc. Natl. Acad. Sci. USA* **113**, 2642–2647.
- Lupas, A., Baumeister, W., and Hofmann, K. (1997). A repetitive sequence in subunits of the 26S proteasome and 20S cyclosome (APC). *Trends Biochem. Sci.* **22**, 195–196.
- Mansour, W., Nakasone, M.A., von Delbruck, M., Yu, Z., Krutauz, D., Reis, N., Kleefeld, O., Sommer, T., Fushman, D., and Glickman, M.H. (2015). Disassembly of Lys11 and mixed linkage polyubiquitin conjugates provides insights into function of proteasomal deubiquitinases Rpn11 and Ubp6. *J. Biol. Chem.* **290**, 4688–4704.
- Matiuhin, Y., Kirkpatrick, D.S., Ziv, I., Kim, W., Dakshinamurthy, A., Kleefeld, O., Gygi, S.P., Reis, N., and Glickman, M.H. (2008). Extraproteasomal Rpn10 restricts access of the polyubiquitin-binding protein Dsk2 to proteasome. *Mol. Cell* **32**, 415–425.
- Matyskiela, M.E., Lander, G.C., and Martin, A. (2013). Conformational switching of the 26S proteasome enables substrate degradation. *Nat. Struct. Mol. Biol.* **20**, 781–788.
- Mayor, T., Sharon, M., and Glickman, M.H. (2016). Tuning the proteasome to brighten the end of the journey. *Am. J. Physiol. Cell Physiol.* **311**, C793–C804.
- Meyer, H.J., and Rape, M. (2014). Enhanced protein degradation by branched ubiquitin chains. *Cell* **157**, 910–921.
- Miller, S.L.H., Malotky, E., and O'Bryan, J.P. (2004). Analysis of the role of UIMs in ubiquitin-binding and ubiquitylation. *J. Biol. Chem.* **279**, 33528–33537.
- Mueller, T., and Feigon, J. (2003). Structural determinants for the binding of ubi domains to the proteasome. *EMBO J.* **22**, 4634–4645.
- Mueller, T.D., Kamionka, M., and Feigon, J. (2004). Specificity of the interaction between ubiquitin-associated domains and ubiquitin. *J. Biol. Chem.* **279**, 11926–11936.
- Nakasone, M.A., Livnat-Levanon, N., Glickman, M.H., Cohen, R.E., and Fushman, D. (2013). Mixed-linkage ubiquitin chains send mixed messages. *Structure* **21**, 727–740.
- Nathan, J.A., Kim, H.T., Ting, L., Gygi, S.P., and Goldberg, A.L. (2013). Why do cellular proteins linked to K63-polyubiquitin chains not associate with proteasomes? *EMBO J.* **32**, 552–565.
- Nowicka, U., Zhang, D., Walker, O., Krutauz, D., Castaneda, C.A., Chaturvedi, A., Chen, T.Y., Reis, N., Glickman, M.H., and Fushman, D. (2015). DNA-damage-inducible 1 protein (Ddi1) contains an uncharacteristic ubiquitin-like domain that binds ubiquitin. *Structure* **23**, 542–557.
- Ohno, A., Jee, J., Fujiwara, K., Tenno, T., Goda, N., Tochio, H., Kobayashi, H., Hiroaki, H., and Shirakawa, M. (2005). Structure of the UBA domain of Dsk2p in complex with ubiquitin molecular determinants for ubiquitin recognition. *Structure* **13**, 521–532.
- Paraskevopoulos, K., Kriegenburg, F., Tatham, M.H., Rosner, H.I., Medina, B., Larsen, I.B., Brandstrup, R., Hardwick, K.G., Hay, R.T., Kragelund, B.B., et al. (2014). Dss1 is a 26S proteasome ubiquitin receptor. *Mol. Cell* **56**, 453–461.
- Pathare, G.R., Nagy, I., Sledz, P., Anderson, D.J., Zhou, H.J., Pardon, E., Steyaert, J., Forster, F., Bracher, A., and Baumeister, W. (2014). Crystal structure of the proteasomal deubiquitylation module Rpn8-Rpn11. *Proc. Natl. Acad. Sci. USA* **111**, 2984–2989.
- Peth, A., Besche, H.C., and Goldberg, A.L. (2009). Ubiquitinated proteins activate the proteasome by binding to Usp14/Ubp6, which causes 20S gate opening. *Mol. Cell* **36**, 794–804.
- Peth, A., Kukushkin, N., Bosse, M., and Goldberg, A.L. (2013a). Ubiquitinated proteins activate the proteasomal ATPases by binding to Usp14 or Uch37 homologs. *J. Biol. Chem.* **288**, 7781–7790.
- Peth, A., Nathan, J.A., and Goldberg, A.L. (2013b). The ATP costs and time required to degrade ubiquitinated proteins by the 26 S proteasome. *J. Biol. Chem.* **288**, 29215–29222.
- Pettersen, E.F., Goddard, T.D., Huang, C.C., Couch, G.S., Greenblatt, D.M., Meng, E.C., and Ferrin, T.E. (2004). UCSF Chimera—a visualization system for exploratory research and analysis. *J. Comput. Chem.* **25**, 1605–1612.
- Pickart, C.M., and Fushman, D. (2004). Polyubiquitin chains: polymeric protein signals. *Curr. Opin. Chem. Biol.* **8**, 610–616.
- Raasi, S., Orlov, I., Fleming, K.G., and Pickart, C.M. (2004). Binding of polyubiquitin chains to ubiquitin-associated (UBA) domains of HHR23A. *J. Mol. Biol.* **341**, 1367–1379.
- Raasi, S., Varadan, R., Fushman, D., and Pickart, C.M. (2005). Diverse polyubiquitin interaction properties of ubiquitin-associated domains. *Nat. Struct. Mol. Biol.* **12**, 708–714.
- Rahighi, S., and Dikic, I. (2012). Selectivity of the ubiquitin-binding modules. *FEBS Lett.* **586**, 2705–2710.
- Riedinger, C., Boehringer, J., Trempe, J.F., Lowe, E.D., Brown, N.R., Gehring, K., Noble, M.E., Gordon, C., and Endicott, J.A. (2010). Structure of Rpn10 and its interactions with polyubiquitin chains and the proteasome subunit Rpn12. *J. Biol. Chem.* **285**, 33992–34003.
- Rosenzweig, R., Bronner, V., Zhang, D., Fushman, D., and Glickman, M.H. (2012). Rpn1 and Rpn2 coordinate ubiquitin processing factors at proteasome. *J. Biol. Chem.* **287**, 14659–14671.
- Saeki, Y., Kudo, T., Sone, T., Kikuchi, Y., Yokosawa, H., Toh-e, A., and Tanaka, K. (2009). Lysine 63-linked polyubiquitin chain may serve as a targeting signal for the 26S proteasome. *EMBO J.* **28**, 359–371.
- Sakata, E., Bohn, S., Mihalache, O., Kiss, P., Beck, F., Nagy, I., Nickell, S., Tanaka, K., Saeki, Y., Forster, F., et al. (2012). Localization of the proteasomal ubiquitin receptors Rpn10 and Rpn13 by electron cryomicroscopy. *Proc. Natl. Acad. Sci. USA* **109**, 1479–1484.
- Schreiner, P., Chen, X., Husnjak, K., Randles, L., Zhang, N.X., Elsasser, S., Finley, D., Dikic, I., Walters, K.J., and Groll, M. (2008). Ubiquitin docking at

the proteasome through a novel pleckstrin-homology domain interaction. *Nature* 453, 548–552.

Schweitzer, A., Aufderheide, A., Rudack, T., Beck, F., Pfeifer, G., Plitzko, J.M., Sakata, E., Schulten, K., Forster, F., and Baumeister, W. (2016). Structure of the human 26S proteasome at a resolution of 3.9 Å. *Proc. Natl. Acad. Sci. USA* 113, 7816–7821.

Scott, D., Oldham, N.J., Strachan, J., Searle, M.S., and Layfield, R. (2015). Ubiquitin-binding domains: mechanisms of ubiquitin recognition and use as tools to investigate ubiquitin-modified proteomes. *Proteomics* 15, 844–861.

Sharon, M., Taverner, T., Ambroggio, X.I., Deshaies, R.J., and Robinson, C.V. (2006). Structural organization of the 19S proteasome lid: insights from MS of intact complexes. *PLoS Biol.* 4, e267.

Shi, Y., Chen, X., Elsasser, S., Stocks, B.B., Tian, G., Lee, B.H., Shi, Y., Zhang, N., de Poot, S.A., Tuebing, F., et al. (2016). Rpn1 provides adjacent receptor sites for substrate binding and deubiquitination by the proteasome. *Science* 351, <http://dx.doi.org/10.1126/science.aad9421>.

Sims, J.J., and Cohen, R.E. (2009). Linkage-specific avidity defines the lysine 63-linked polyubiquitin-binding preference of rap80. *Mol. Cell* 33, 775–783.

Sims, J.J., Haririnia, A., Dickinson, B.C., Fushman, D., and Cohen, R.E. (2009). Avid interactions underlie the Lys63-linked polyubiquitin binding specificities observed for UBA domains. *Nat. Struct. Mol. Biol.* 16, 883–889.

Singh, R.K., Zerath, S., Kleifeld, O., Scheffner, M., Glickman, M.H., and Fushman, D. (2012). Recognition and cleavage of related to ubiquitin 1 (Rub1) and Rub1-ubiquitin chains by components of the ubiquitin-proteasome system. *Mol. Cell Proteomics* 11, 1595–1611.

Singh, S.K., Sahu, I., Mali, S.M., Hemantha, H.P., Kleifeld, O., Glickman, M.H., and Brik, A. (2016). Synthetic uncleavable ubiquitinated proteins dissect proteasome deubiquitination and degradation, and highlight distinctive fate of tetraubiquitin. *J. Am. Chem. Soc.* 138, 16004–16015.

Sledz, P., Forster, F., and Baumeister, W. (2013a). Allosteric effects in the regulation of 26S proteasome activities. *J. Mol. Biol.* 425, 1415–1423.

Sledz, P., Unverdorben, P., Beck, F., Pfeifer, G., Schweitzer, A., Forster, F., and Baumeister, W. (2013b). Structure of the 26S proteasome with ATP- γ S bound provides insights into the mechanism of nucleotide-dependent substrate translocation. *Proc. Natl. Acad. Sci. USA* 110, 7264–7269.

Tugarinov, V., Kanelis, V., and Kay, L.E. (2006). Isotope labeling strategies for the study of high-molecular-weight proteins by solution NMR spectroscopy. *Nat. Protoc.* 1, 749–754.

Unverdorben, P., Beck, F., Sledz, P., Schweitzer, A., Pfeifer, G., Plitzko, J.M., Baumeister, W., and Forster, F. (2014). Deep classification of a large cryo-EM dataset defines the conformational landscape of the 26S proteasome. *Proc. Natl. Acad. Sci. USA* 111, 5544–5549.

Varadan, R., Walker, O., Pickart, C., and Fushman, D. (2002). Structural properties of polyubiquitin chains in solution. *J. Mol. Biol.* 324, 637–647.

Varadan, R., Assfalg, M., Haririnia, A., Raasi, S., Pickart, C., and Fushman, D. (2004). Solution conformation of Lys63-linked di-ubiquitin chain provides clues to functional diversity of polyubiquitin signaling. *J. Biol. Chem.* 279, 7055–7063.

Varadan, R., Assfalg, M., Raasi, S., Pickart, C., and Fushman, D. (2005). Structural determinants for selective recognition of a Lys48-linked polyubiquitin chain by a UBA domain. *Mol. Cell* 18, 687–698.

Verma, R., Chen, S., Feldman, R., Schieltz, D., Yates, J., Dohmen, J., and Deshaies, R.J. (2000). Proteasomal proteomics: identification of nucleotide-sensitive proteasome-interacting proteins by mass spectrometric analysis of affinity-purified proteasomes. *Mol. Biol. Cell* 11, 3425–3439.

Verma, R., Aravind, L., Oania, R., McDonald, W.H., Yates, J.R., 3rd, Koonin, E.V., and Deshaies, R.J. (2002). Role of Rpn11 metalloprotease in deubiquitination and degradation by the 26S proteasome. *Science* 298, 611–615.

Volk, S., Wang, M., and Pickart, C.M. (2005). Chemical and genetic strategies for manipulating polyubiquitin chain structure. *Methods Enzymol.* 399, 3–20.

Wang, Z.X. (1995). An exact mathematical expression for describing competitive binding of two different ligands to a protein molecule. *FEBS Lett.* 360, 111–114.

Wang, B., Matsuoka, S., Ballif, B.A., Zhang, D., Smogorzewska, A., Gygi, S.P., and Elledge, S.J. (2007). Abraxas and RAP80 form a BRCA1 protein complex required for the DNA damage response. *Science* 316, 1194–1198.

Wilkinson, C.R., Seeger, M., Hartmann-Petersen, R., Stone, M., Wallace, M., Semple, C., and Gordon, C. (2001). Proteins containing the UBA domain are able to bind to multi-ubiquitin chains. *Nat. Cell Biol.* 3, 939–943.

Winget, J.M., and Mayor, T. (2011). The diversity of ubiquitin recognition: hot spots and varied specificity. *Mol. Cell* 38, 627–635.

Worden, E.J., Padovani, C., and Martin, A. (2014). Structure of the Rpn11-Rpn8 dimer reveals mechanisms of substrate deubiquitination during proteasomal degradation. *Nat. Struct. Mol. Biol.* 21, 220–227.

Yu, Z., Livnat-Levanon, N., Kleifeld, O., Mansour, W., Nakasone, M.A., Castaneda, C.A., Dixon, E.K., Fushman, D., Reis, N., Pick, E., et al. (2015). Base-CP proteasome can serve as a platform for stepwise lid formation. *Biosci. Rep.* 35, e00194.

Yun, J.H., Ko, S., Lee, C.K., Cheong, H.K., Cheong, C., Yoon, J.B., and Lee, W. (2013). Solution structure and Rpn1 interaction of the UBL domain of human RNA polymerase II C-terminal domain phosphatase. *PLoS One* 8, e62981.

Zhang, D., Raasi, S., and Fushman, D. (2008). Affinity makes the difference: nonselective interaction of the UBA domain of Ubiquitin-1 with monomeric ubiquitin and polyubiquitin chains. *J. Mol. Biol.* 377, 162–180.

Zhang, D., Chen, T., Ziv, I., Rosenzweig, R., Matiuhi, Y., Bronner, V., Glickman, M.H., and Fushman, D. (2009a). Together, Rpn10 and Dsk2 can serve as a polyubiquitin chain-length sensor. *Mol. Cell* 36, 1018–1033.

Zhang, N., Wang, Q., Ehlinger, A., Randles, L., Lary, J.W., Kang, Y., Haririnia, A., Storaska, A.J., Cole, J.L., Fushman, D., et al. (2009b). Structure of the s5a:k48-linked diubiquitin complex and its interactions with rpn13. *Mol. Cell* 35, 280–290.

Zhou, L., Holt, M.T., Ohashi, N., Zhao, A., Muller, M.M., Wang, B., and Muir, T.W. (2016). Evidence that ubiquitylated H2B corals hDot1L on the nucleosomal surface to induce H3K79 methylation. *Nat. Commun.* 7, 10589.

STAR★METHODS

KEY RESOURCES TABLE

REAGENT or RESOURCE	SOURCE	IDENTIFIER
Antibodies		
α -Sc.RAD23	Glickman lab	
α -RGS	Qiagen	Cat# 34610
α -RPN1	This work	
α -RPN10	Glickman lab	
α -RPN12	Glickman lab	
α -UB	DAKO	Cat# Z0458
α K48 PolyUb	Millipore	Cat# 05-1307
α K63 PolyUb	Millipore	Cat# 05-1308
α -Chicken HRP	Chemicon	Cat# AP162P
α -Mouse HRP	Jackson	Cat# 115-035-062
α -Rabbit HRP	Biorad	Cat# 1706515
Bacterial Strains		
DH5a	Glickman's lab	
M15	Glickman's lab	Qiagen
Rosetta (BL21)	Fushman's lab	Novagene
Biological Samples		
Yeast proteasomes	This work	http://dx.doi.org/10.1016/S0092-8674(00)81603-7
Chemicals, Peptides, and Recombinant Proteins		
L-2-amino-4,4-azido-pentanoic acid (l-photoleucine)	Thermo Scientific	Cat#22610
SPPS reagents - Fmoc amino acids, PyBOP, special dipeptides	El Qualid et al., 2010, Novabiochem	http://dx.doi.org/10.1002/anie.201005995
Acetonitrile, HPLC-R grade	Biosolve	Cat#01201304, CAS#75-05-8
Trifluoroacetic acid, peptide synthesis grade	Biosolve	Cat#20233332, CAS#76-05-1
N-Methyl-2-Pyrrolidone, peptide synthesis grade	Biosolve	Cat#13563202, CAS#872-50-4
Piperidine, peptide synthesis grade	Biosolve	CAT#16183301, CAS#110-89-4
N,N-Dimethylformamide, AR grade	Biosolve	CAT#04190501, CAS#68-12-2
Formic acid, ULC/MS grade	Biosolve	CAT#06914143, CAS#64-18-6
N-(9-Fluorenylmethoxycarbonyloxy)succinimide	Chem-Impex	CAT#00147, CAS#82911-69-1
Methanol, AR grade	Biosolve	CAT#13680502, CAS#67-56-1
Dichloromethane, AR grade	Biosolve	CAT#13790502, CAS#75-09-2
Tetrahydrofuran, AR grade	Biosolve	CAT#20630502, CAS#109-99-9
Ethylacetate, AR grade	Biosolve	CAT#05400502, CAS#141-78-6
DMSO, AR grade	Biosolve	CAT#04470501, CAS#67-68-5
Sodium carbonate, anhydrous	Fluka	CAT#71352, CAS#497-19-8
Hydrochloric acid, reagent grade, 37%	Sigma-Aldrich	CAT#435570, CAS#7647-01-0
Chloroform D, NMR, 99.8%	Euriso-Top	CAT#D007H, CAS#865-49-6
Acrylamide/bis 37.5:1	Sigma	CAT#A7168
Acrylamide/bis 19:1	Sigma	CAT#A9926
Adenosine 5' triphosphate (ATP)	Calbiochem	CAT#1191
Alexa Flour 488 C5 Maleamide	Thermo-Fisher	CAT#A20347
Dithiothreitol (DTT)	Calbiochem	CAT#233155
Kanamycin	Sigma	CAT#K4000
Ampicillin	Sigma	CAT#A9518
Isopropyl β -D-1-thiogalactopyranoside (IPTG)	Sigma	CAT#I6758

(Continued on next page)

Continued

REAGENT or RESOURCE	SOURCE	IDENTIFIER
Potassium Chloride	Carlo Erba	CAT#471177
Potassium Phosphate dihydrate	Merck	CAT#1.04873
Potassium Phosphate dibasic	Spectrum	CAT#P1383
Sodium chloride	Bio-Lab	CAT#19030591
Trizma-base	Sigma	CAT#T1503
Glycerol	Bio-Lab	CAT#07120501
HEPES	Fisher Bioreagents	CAT#BP310
Imidazole	Alfa Aesar	CAT#10221
Tris 2-carboxyethyl phosphine (TCEP)	GoldBio	CAT#51805-45-9
Rpn1 derivatives purified proteins	This work	
UB derivatives purified proteins	This work	
UB Chains purified proteins	This work	
Recombinant DNA Plasmids		
pET28b-RPN10	Glickman's lab	M83
pET28b-SMT3	Ariel Stanhill lab	DOI: 10.1110/ps.035188.108
pET28b-SMT3-RPN1	This work	M1292
pET28b-SMT3-RPN1 ⁴¹⁶⁻⁴⁸⁷	This work	M1433
pET28b-SMT3-RPN1 ^{905-end}	This work	M1272
pET28b-SMT3-RPN1 ³⁹¹⁻⁶⁴²	This work	M1548
pET28b-SMT3-RPN1 ³⁵⁶⁻⁹⁰⁵	This work	M1373
pET28b-SMT3-RPN12	This work	M1257
Ub plasmids, E1, E2	Nakasone et al., 2013 Structure 21(5)	http://dx.doi.org/10.1016/j.str.2013.02.019
DSK2 and RPN10	Zhang et al., 2009a . Mol.Cell 36(6)	https://dx.doi.org/10.1016/j.molcel.2009.11.012
RAP80 tUIM	Nakasone et al., 2013 Structure 21(5)	http://dx.doi.org/10.1016/j.str.2013.02.019
pQE30-UBP6 C118A	Mansour et al., 2015 JBC 290(8)	DOI 10.1074/jbc.M114.568295
Software and Algorithms		
LCMS analysis - MassLynx 4.1	Waters	NA
NMR analysis - Topspin 3.2	Bruker	NA

CONTACT FOR REAGENT AND RESOURCE SHARING

Further information and requests for reagents can be directed to the leading author: Michael H. Glickman (gllickman@tx.technion.ac.il).

EXPERIMENTAL MODEL AND SUBJECT DETAILS

Proteasome was purified from widely used laboratory yeast strain, BY4741 obtained from EUROSCARF (MATa his3Δ1 leu2Δ0 met15Δ0 ura3Δ0), considered in this study as “wild-type” yeast.

All recombinant proteins were cloned from cDNA isolated from BY4741 yeast and expressed in E. coli (either M15, BL21(DE3) or Rosetta (II)).

METHOD DETAILS

Plasmid Construction and Protein Purification

Smt3 (SUMO) was ligated into the pET28b vector. Subsequently, the full-length Rpn1 DNA sequence was amplified from yeast genomic DNA and ligated in the smt3-pET28b vector, downstream of smt3. Shorter fragments, Rpn1⁴¹⁶⁻⁴⁸⁷, Rpn1⁹⁰⁵⁻⁹⁹³, Rpn1³⁹¹⁻⁶⁴², and Rpn1³⁵⁶⁻⁹⁰⁵ were created by applying the appropriate primer pair to the full length Rpn1 for ligation into the

smt3-pET28b vector. All ligations were performed using T4 DNA fast ligase (Promega) according to the manufacturer's protocol. Ligation products were transformed into chemically competent *E. coli* DH5 α (Life technologies) cells and selected against 50 μ g/mL kanamycin. Plasmids were extracted and sequenced from the forward and reverse directions to confirm their integrity. Full length Rpn12 was ligated into the same smt3-pET28b vector. Plasmids for other proteins used have been reported in previous studies; Rpn10 and DSK2 variants (Zhang et al., 2009a), Rap80-tUIM (Nakasone et al., 2013), Rad23 constructs (Rosenzweig et al., 2012), Rub1 (Singh et al., 2012), and Ubp6^{C118A} (Mansour et al., 2015).

Proteins in pQE30 vectors were expressed in *E. coli* M15 cells (Novagen), while those in pET28b were expressed in BL-21 (DE3) Rosetta II cells (Novagen). 2 L cultures of LB media supplemented with the respective antibiotic (pQE30 100 μ g/mL ampicillin or pET28b 50 μ g/mL kanamycin) were grown to OD₆₀₀~0.6 at 37°C, induced with 0.5 mM Isopropyl β -D-1-thiogalactopyranoside (IPTG), and expression was carried out for 18 hrs at 16°C. Cells were harvested and stored at -80°C until purification. Cells were resuspended in HisTrap buffer A (20 mM phosphate, 200 mM NaCl, 10 mM imidazole, pH 7.4) buffer and lysed using French Press. The lysate was cleared with centrifugation, syringe filtered and loaded on to a pre-equilibrated 10 mL HisTrap (GE Life Sciences) column in the same buffer. Proteins were eluted using steps of 5 column volumes 10% and 70% HisTrap buffer B (20 mM phosphate, 200 mM NaCl, 280 mM imidazole, pH 7.4). Following elution, fractions containing proteins of interest were pooled and dialyzed against PBS pH 7.4 buffer. To obtain the highest purity, gel filtration was performed using a Superdex 200 16/60 (GE Life Sciences) in PBS pH 7.4 buffer. Purity was confirmed with SDS-PAGE and proteins were aliquoted and stored at -80 °C.

Purification of Rpn1 and Rpn1 Fragments

Cell pellets expressing His₆-Smt3-Rpn1 and fragments were suspended in HisTrap buffer A (50 mM HEPES pH 7.5, 400 mM KCl, 2.5% glycerol, 10 mM imidazole and 5 mM β -ME) and lysed using a French press. The cellular debris were cleared by centrifugation and the supernatant was loaded onto a 10 mL HisTrap column in the same buffer. Elution was performed with HisTrap buffer B (50 mM HEPES pH 7.5, 400 mM KCl, 2.5% glycerol, 280 mM imidazole and 5 mM β -ME) in two 5 cv steps, 10% then 70%. ¹³CH₃-ILVM labeled Rpn1 constructs were obtained following (ref Kay – see section below) and purified in the same as above, except that the HisTrap buffers were changed to HisTrap buffer A (50 mM Tris pH 8.0, 300 mM KCl, 10 mM imidazole) for loading, and HisTrap buffer B (50 mM Tris pH 8.0, 500 mM KCl, 250 mM imidazole) for elution. Fractions containing Rpn1 were detected using SDS-PAGE, pooled and dialyzed at 4°C against (40 mM HEPES pH8, 250 mM KCl and 5 mM β -ME) or 50 mM Hepes pH 7.6, 500 mM KCl, 5 mM DTT, 5% glycerol for ¹³CH₃-ILVM-Rpn1. In the respective buffers, the His₆-smt3 tag was removed from Rpn1 constructs using His₆-ULP1 and the desired Rpn1 constructs were isolated using Ni-NTA resin. To obtain the appropriated oligomeric state and purity, Rpn1 constructs were then injected on a Superdex S75 16/60 column in 20 mM HEPES pH 8.0, 100 mM KCl and 2.5% glycerol or 50 mM Hepes pH 7.6, 500 mM KCl, 2 mM TCEP for ¹³CH₃-ILVM-Rpn1.

Methyl Labelling Rpn1^{PC1}

Cells were grown at 37°C in M9 D₂O media supplemented with ¹⁴NH₄Cl and [²H,¹²C]-glucose as the sole nitrogen and carbon sources, respectively. Methyl labeling of the Ile- δ 1-[¹³CH₃] and Val/Leu-[¹³CH₃, ¹²CD₃] variety (referred to as ILV-protein in what follows, that is U-[¹⁵N,²H], Ile δ 1-[¹³CH₃], Leu,Val-[¹³CH₃, ¹²CD₃]-labeled) followed a published procedure (Tugarinov et al., 2006).

Assembly of K48- and K63-Linked polyUb^{PT(8)} and polyUb^{PT(738)} Chains

Monomeric Ub mutants, E2 conjugating enzymes, and human E1 were obtained recombinantly as described (Nakasone et al., 2013; Volk et al., 2005). Enzymatically synthesized K48-, and K63-linked Ub chains were assembled by combining a proximally blocked Ub mutant (Ub-His₆) in combination with pLeu8 or pLeu73 modified Ub (Castaneda et al., 2013; Nakasone et al., 2013). K48-linked Ub chains were obtained from a reaction containing 1 mg of Ub-His₆ and 10 mg of each Ub^{PT(8)} or Ub^{PT(73)}, 80 nM E1 (UBA1), 40 μ M E2-25K, 4 mM TCEP, and 15 mM ATP in a volume of 1 mL with a 50 mM Tris pH 8.0 buffer incubated at 37 °C for 20 hours. In a similar fashion, reactions to generate K63-linked Ub chains contained 30 μ M of each Ubc13 and Uev1a with same monomers in addition to 50 ng of Ub^{K63R} to influence chain length. Following the completion of each reaction, Ub-His₆ chains were diluted into a volume of 40 mL HisTrap buffer A (20 mM phosphate, 200 mM NaCl, 10 mM imidazole, pH 7.4), and loaded onto a 5 mL HisTrap column. Side products of the reaction flowed through the columns and polyUb^{PT} chains with Ub-His₆ in the proximal position were eluted in HisTrap buffer B (20 mM phosphate, 200 mM NaCl, 280 mM imidazole, pH 7.4). PolyUb^{PT} reactions without Ub-His₆ were first passed through a 1 mL GST column in PBS pH 7.4 buffer to remove E1 and E2 enzymes. Defined polymers of polyUb^{PT} were resolved on a Superdex 75 16/60 size exclusion column (GE Life Sciences) in PBS, pH 7.4. Fractions containing the desired chain lengths were confirmed with SDS-PAGE and stored at -20°C until needed. We note that each step of polyUb^{PT} was carried out in the dark to preserve the crosslinking group.

Yeast Proteasome Purification

Highly pure yeast 26S proteasome obtained from yeast in stationary phase in a total of 6L YPD media, following established protocol (Glickman and Coux, 2001). The activity and structure (RP₂CP) of proteasomes was confirmed using the Suc-LLVY-AMC peptidase activity assay. Proteasome concentration was determined by Bradford assay (Thermo Scientific). Proteasomes were flash frozen in liquid nitrogen and stored at -80°C until use.

Western Blot Analysis

Samples from UV crosslinking reactions were taken and the indicated time point and mixed with 5xPLD for SDS-PAGE. Gels were transferred to nitrocellulose membranes (GE Life Sciences), blocked in 5% (w/v) non-fat milk for 1 hour at room temperature, washed and incubated with the primary antibody for 1 hour at room temperature (see [Key Resources Table](#)). Membranes were then washed and incubated with the respective secondary HRP conjugate antibody (Bio-Rad) for chemiluminescence analysis with an Image Quant LAS 4000 (GE Healthcare).

Assembly of Ub₂ Chains for NMR Measurements

K48-linked and K63-linked diUb with ¹⁵N-enriched distal Ub were assembled using chain-termination mutations (K48R or K63R on the distal Ub and D77 on the proximal) as described ([Varadan et al., 2002, 2004](#)). K48-linked diUb with heavy isotope labeling ¹³C-ILVM on both ubiquitin units were assembled using E1 and E2-25K enzymes and ILVM-labeled monoUb; the dimers were separated from the rest of the reaction products using cation exchange chromatography followed by size exclusion.

NMR Measurements

NMR-based titration assays were performed by monitoring changes in NMR spectra of isotope-labeled component (protein) upon addition of unlabeled binding partner (ligand). The K_D values were derived from a global fit model that provides errors based on the fit calculated by a nonlinear least square fit to a single-site binding model using the equation:

$$\Delta\delta = \Delta\delta_{\text{MAX}} \frac{[P]_T + [L]_T + K_D - \sqrt{([P]_T + [L]_T + K_D)^2 - 4[P]_T[L]_T}}{2[P]_T}$$

where [P]_T and [L]_T are the total protein and ligand concentrations at each titration point, Δδ is the change in peak position from the apo state and Δδ_{MAX} is the chemical shift difference between apo and fully bound states of the protein ([Varadan et al., 2004](#)). For ¹³C measurements, binding isotherms were quantified separately for ¹H or ¹³C chemical shifts with Δδ calculated from the following relation:

$$\Delta\delta = \sqrt{\left(\frac{\Delta\delta_H}{\alpha}\right)^2 + \left(\frac{\Delta\delta_C}{\beta}\right)^2} \quad (\text{Equation 2})$$

where Δδ_{H(C)} is the shift change between methyl group ¹H (¹³C) nuclei in apo and fully saturated forms of the protein, α (β) is one standard deviation of the methyl ¹H (¹³C) chemical shifts (separate values of α (β) are used for different methyl groups), as tabulated in the Biological Magnetic Resonance Databank (www.bmrb.wisc.edu). For ¹⁵N measurements, combined chemical shift perturbations were used, calculated as follows: Δδ = √(Δδ_H² + 0.04Δδ_N²), where Δδ_H and Δδ_N are shifts in ¹H and ¹⁵N resonances, respectively.

¹⁵N relaxation rates were measured using standard methods as described ([Hall and Fushman, 2003](#)).

Ub^{PT} Crosslinking Conditions

The crosslink reaction was performed in 96 well-plates, allowing for a 30 minute preincubation at 30°C. Samples were placed 10 cm from the light source and UV-irradiated for 30 min using 5X8W UV Bulbs 302/355 nm (Cleaver Scientific – UV Crosslinker). Rad23 competition reactions were conducted in PBS pH 7.4 buffer using 1 μM of Rpn1^{PC}, 5 μM K48-Ub₄₊^{PT(73)}, and 0.5 μM or 1 μM of Rad23. Proteasome crosslinking was carried out in 25 mM Tris pH 7.4, 10 mM MgCl₂, 10% glycerol, 2 mM ATP and 1 mM DTT buffer. 200 nM proteasome was first pre-incubated with 0.1 mM NEM for 30 minutes. UV Crosslinking occurred after addition of 400 nm Rad23 and 2 μM of the indicated polyUb₄₊^{PT}.

Docking Simulations and Bioinformatics Analysis

pyDockWEB

Docking analysis were done with pyDockWeb ([Jimenez-Garcia et al., 2013](#)), a web tool for the structural prediction of protein-protein interactions. Given the 3D coordinates of two interacting proteins (which can be modeled or experimental PDB structures), pyDockWEB returns the best rigid-body docking orientations generated by FTDock ([Gabb et al., 1997](#)) and evaluated by pyDock scoring function ([Cheng et al., 2007](#)), which includes electrostatics, desolvation and limited van der Waals contribution energy terms.

NIP Method

Normalized interface propensity (NIP) values derived from rigid body docking with electrostatics and desolvation scoring for the prediction of interaction hotspots ([Grosdidier et al., 2007](#)). The ensembles of the rigid-body docking solutions generated by the simulations were subsequently used to project the docking energy landscapes onto the protein surfaces. Highly populated low-energy regions consistently correspond to actual binding sites. Most of the predicted hot-spot residues are above NIP values of 0.3.

ConSurf Server

The ConSurf server ([Glaser et al., 2003](#)) is a bioinformatics tool for estimating the evolutionary conservation of amino positions in a protein molecule based on the phylogenetic relationships between homologous sequences. The degree to which an amino (or nucleic) acid position is evolutionarily conserved is strongly dependent on its structural and functional importance; rapidly evolving

positions are variable while slowly evolving positions are conserved. Thus, conservation analysis of positions among members from the same family can often reveal the importance of each position for the protein structure or function.

UCSF Chimera

Molecular graphics and analyses were performed with the UCSF Chimera package. Chimera is developed by the Resource for Bio-computing, Visualization, and Informatics at the University of California, San Francisco (<http://www.cgl.ucsf.edu/chimera>) supported by NIGMS P41-GM103311). (Pettersen et al., 2004)

Chemical Methods Synthesis of Monomeric Ub^{PT(8)} and Ub^{PT(73)}

All commercial materials (Aldrich, Fluka, Novabiochem, Biosolve, Thermo Scientific) were used without further purification. L-2-amino-4,4-azido-pentanoic acid (L-photoleucine) was purchased from Thermo Scientific. Peptide synthesis reagents (standard amino acid building blocks and PyBop) were purchased from Novabiochem. All solvents were reagent grade or HPLC grade. Unless stated otherwise, reactions were performed under an inert atmosphere. NMR spectra (¹H and ¹³C) were recorded on a Bruker Avance 300 spectrometer, referenced to TMS or residual solvent. LC-MS analysis was performed on a system equipped with a Waters 2795 separation Module (Alliance HT), Waters 2996 Photodiode Array Detector (190–750 nm), Phenomenex KinetexTM C18 (100A, 100 x 21 mm, 2.6 μm) reversed phase column or Phenomenex KinetexTM XB-C18 100A (50 x 2 mm, 2.6 μm) reversed phase column and a Micromass LCT-TOF mass spectrometer. Samples were run at 0.40 mL/min using a gradient of two mobile phases, A: 0.1% aq. formic acid and B: 0.1% formic acid in acetonitrile. Data processing was performed using Waters MassLynx 4.1 software. Preparative HPLC was performed on a Waters XBridgeTM Prep C18 Column (30 x 150 mm, 5 μm OBDTM) at a flow rate of 37.5 mL/min. The solvents used were aq. 0.05% TFA (Solvent A) and acetonitrile containing 0.05% TFA (Solvent B) using gradient elution.

Compound Synthesis and Characterization

L-2-amino-4,4-azido-pentanoic acid (L-photoleucine, 100 mg, 0.7 mmol) was dissolved in 5 mL of 10% aq Na₂CO₃. To this, a solution of Fmoc N-hydroxysuccinimide ester (Fmoc-OSu, 1.2 eq, 0.84 mmol, 283 mg) in 5 mL THF was added (Scheme S1). The reaction mixture was stirred overnight at RT. A sample from the reaction mixture was analyzed by LC-MS (LCT, micromass) to determine the formation of Fmoc-photoleucine. LC-MS R_t 7.03 min; MS ES⁺ calculated: 366.39; found 365.93. Phenomenex KinetexTM C18 (100A, 100 x 21 mm, 2.6 μm); solvents - 0.1% aq. formic acid (Solvent A) and acetonitrile containing 0.1% formic acid (Solvent B), flow rate = 0.4 mL/min, runtime = 12 min, column T = 45°C. Gradient: 5% ⇌ 95% solvent B over 7.5 min.

The THF was removed by evaporation under reduced pressure and the remaining aqueous phase washed with ethyl acetate (20 mL). The organic layer was separated and washed with water (20 mL). Both aqueous layers were combined and acidified with 1M aq HCl until the pH dropped between 1 and 2. The product was extracted two times with ethyl acetate. The combined organic layers were dried over sodium sulphate, filtered and evaporated under reduced pressure. After purification by column chromatography (1% → 5% MeOH/DCM), the product was obtained as a colourless oil (yield: 245 mg, 0.67 mmol, 96%, purity: 90 %, according to NMR). This compound can be further purified to 99% by a preparative reversed phase HPLC. ¹H NMR (300 MHz, CDCl₃): δ = 11.23 (s, 1 H), 7.79 (d, J=7.6 Hz, 2 H), 7.67 (d, J=7.6 Hz, 2 H), 7.60 – 7.28 (m, 4 H), 5.66 (d, J=7.56 Hz, 1 H), 4.62 – 4.42 (m, 3 H), 4.29 (t, J=6.9 Hz, 1 H), 2.13 and 1.69 (m, 2H), 1.09 and 0.9 (2s, 3H). See Schemes S1–S10 for supporting information.

Solid Phase Peptide Synthesis of Ub Containing Photoleucine

The synthesis of ubiquitin by solid phase peptide synthesis was carried out according to the previously reported protocol (El Oualid et al., 2010). Ubiquitin with photoleucine incorporated at positions 8 or 73 and ubiquitin containing photoleucine at positions 8 and 73 were synthesized by solid phase peptide synthesis on TentaGel Trt R resin. After acid (TFA) cleavage, the ubiquitin was precipitated in ether, dried and lyophilized. See Schemes S1–S10 for supporting information.

HPLC Purification of Ub Containing Photoleucine

Ubiquitin containing the photoleucine was first dissolved in DMSO. This solution was slowly added to MQ water containing 0.05% TFA and filtered through a GfxO/0.45 μm GHP membrane Acrodisc[®] Premium 25mm syringe filter. The sample was then injected onto a Waters XBridgeTM Prep C18 Column (30 x 150 mm, 5 μm OBDTM) at a flow rate of 37.5 mL/min. The protein was purified with the gradient outlined Table 1 using aq. 0.05% TFA (Solvent A) and acetonitrile containing 0.05% TFA (Solvent B) as eluents.

The retention time for the ubiquitin mutants was approximately 10 minutes. All fractions containing the protein were confirmed by checking the mass using a LC-MS: R_t 2.8 min; Phenomenex KinetexTM XB-C18 100A (50 x 2 x 10 mm, 2.6 μm); solvents - MQ water with 0.1% formic acid (Solvent A) and acetonitrile containing 0.1% formic acid (Solvent B), flow rate = 0.5 mL/min, runtime = 6 min, column T = 45°C. Gradient: 5% ⇌ 95% B over 3.5 min. All samples containing pure protein were pooled and lyophilized. See Schemes S1–S10 for supporting information. See Schemes S1–S10 for detailed information on gradient used in the HPLC purification of the ubiquitin mutants.

Analysis of Purified Ubiquitin Incorporated with Photoleucine

The ubiquitin mutants were dissolved in DMSO to a concentration of 10 mg/mL. 0.2 μL of this sample was resuspended in 10 μL MQ water. To this solution, 5 μL 3x SDS buffer (containing 7.5% 2-mercaptoethanol) was added and the samples were heated at 70°C for 10 minutes. Samples were then loaded on a Nova 12 % Bis-Tris gel and run at 190 V for 47 mins using MES buffer. See Schemes S1–S10 for supporting information.

LC-MS Analysis of the Purified Ubiquitin Containing Photo-Leucine

All purified proteins were confirmed by checking the mass using LC-MS. R_t 4.45 min; Phenomenex Kinetex™ C18 (100A, 100 x 21 mm, 2.6 μ m); solvents – aq. 0.1% formic acid (Solvent A) and acetonitrile containing 0.1% formic acid (Solvent B), flow rate = 0.4 mL/min, runtime = 12 min, column T = 45°C. Gradient: 5% \Rightarrow 95% B over 7.5 min. (purity > 98%). See [Schemes S1–S10](#) for supporting information.

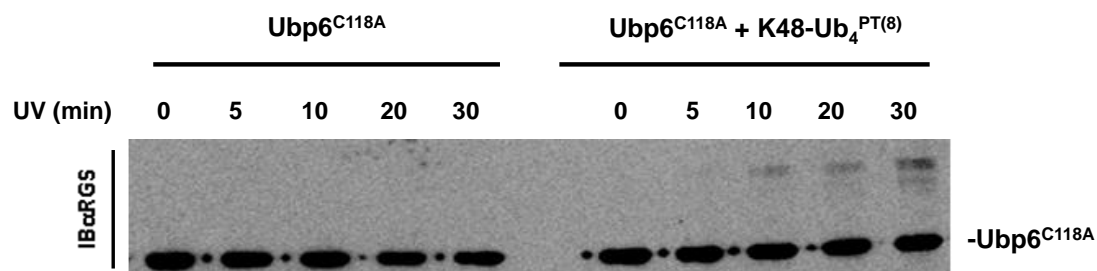
Supplemental Information

Polyubiquitin-Photoactivatable Crosslinking

Reagents for Mapping Ubiquitin Interactome Identify

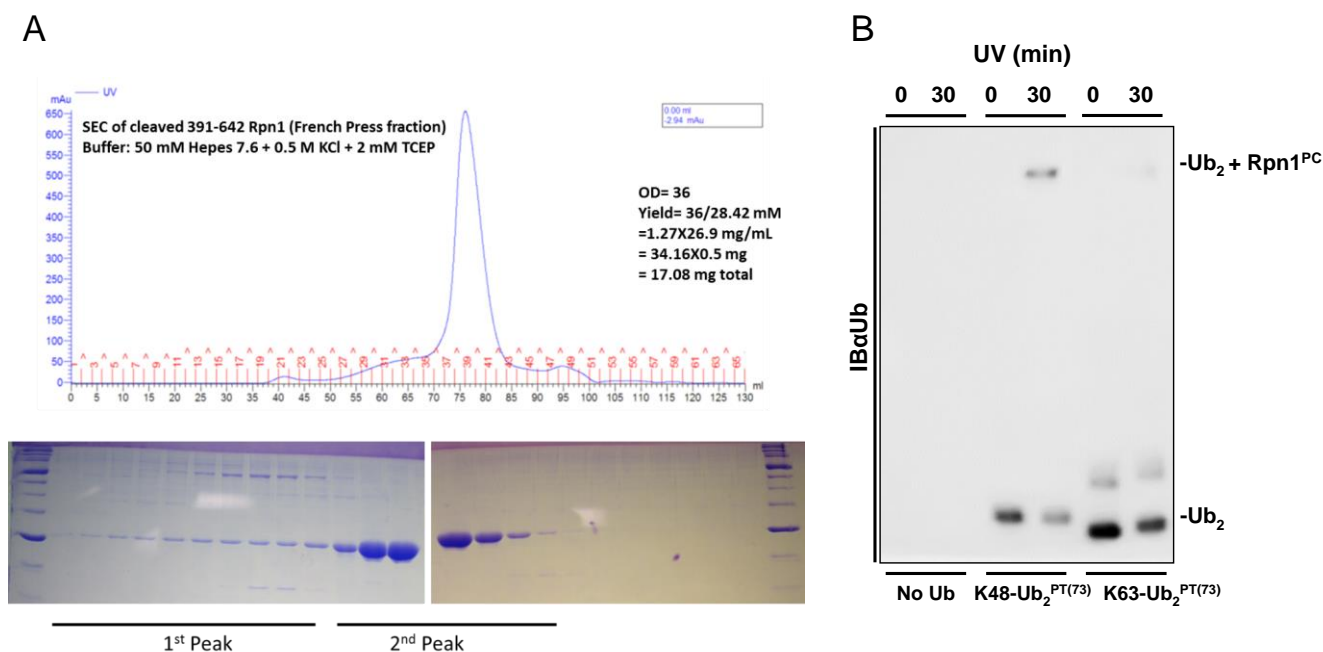
Rpn1 as a Proteasome Ubiquitin-Associating Subunit

Michal Chojnacki, Wissam Mansour, Dharjath S. Hameed, Rajesh K. Singh, Farid El Oualid, Rina Rosenzweig, Mark A. Nakasone, Zanlin Yu, Fabian Glaser, Lewis E. Kay, David Fushman, Huib Ovaa, and Michael H. Glickman



Supplemental Figure S1. Ubp6^{C118A} binding to polyUb^{PT}, related to Figure 3.

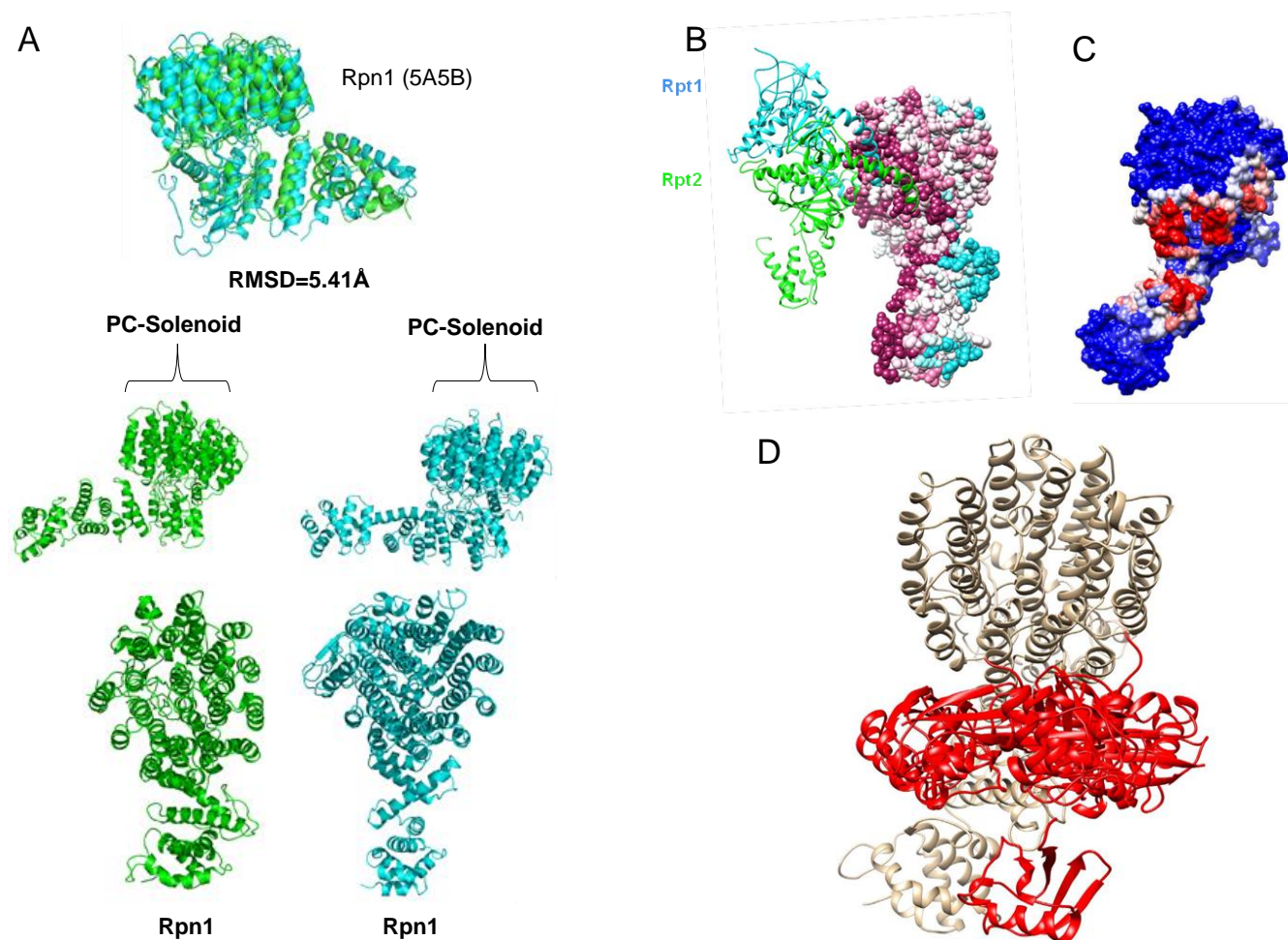
K48-linked polyUb^{PT} crosslinked to purified recombinant Ubp6^{C118A} under similar conditions to those described in Figure 1B.



Supplemental Figure S2. Rpn1 fragments associate with diUb. Related to Figure 4.

A. Truncated Rpn1 fragments, Rpn1⁴¹⁶⁻⁴⁸⁷, Rpn1⁹⁰⁵⁻⁹³³, Rpn1³⁹¹⁻⁶⁴², and Rpn1³⁵⁶⁻⁹⁰⁵ were created by applying the appropriate primer pair to the full length Rpn1 for ligation into the smt3-pET28b vector transformed and expressed in BL-21 (DE3) Rosetta II cells. 2 L cultures were grown to OD₆₀₀~0.6 at 37°C, induced with 0.5 mM Isopropyl β-D-1-thiogalactopyranoside (IPTG), and expression was carried out for 18 hrs. at 16°C. Cell lysate was fractionated first by His-Trap. Following elution, fractions containing Rpn1 fragment were pooled and separated using a Superdex 200 16/60 in PBS pH 7.4 buffer. Rpn1 eluted as sharp peak consistent with uniform behavior of a soluble monomer (top panel). Purity was confirmed with SDS-PAGE (bottom panel). Moreover, Rpn1³⁹¹⁻⁶⁴² migrates at more or less similar position where diUb dimer runs, supporting the conclusion that Rpn1³⁹¹⁻⁶⁴² is soluble as well as monomeric.

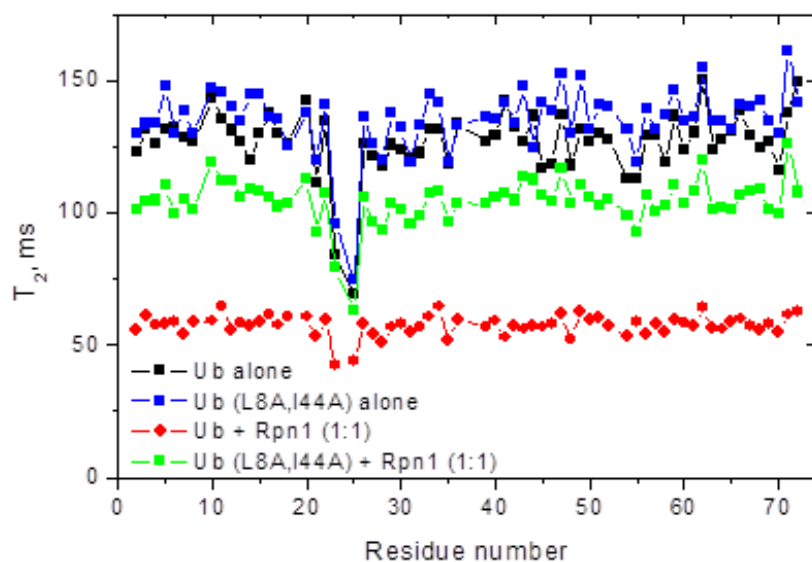
B. Dimeric Ub^{PT} cross-linking with Rpn1³⁵⁶⁻⁹⁰⁵ fragment. K48-linked or K63-linked diUb^{PT} was crosslinked to Rpn1³⁵⁶⁻⁹⁰⁵ fragment according to protocol described in Figure 1B.



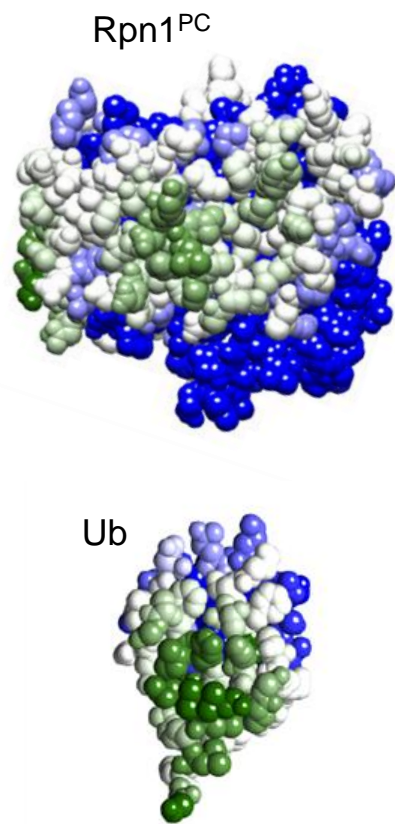
Supplemental Figure S3. Potential protein-protein interaction sites on Rpn1 surface. Related to Figure 4.

A. Alignment of Rpn1 and Rpn2. The structural information from Rpn2 (PDB-4ADY) was effective in locating electron density assigned to Rpn1 in cryoEM-derived proteasome models (5A5B). Rpn1 (green) and Rpn2 (cyan, PDB-4ADY), RMSD=8.60Å. **B. Residue conservation on Rpn1 surface based on current 3D structural Model of Rpn1 in 26S proteasomes.** Evolutionary conservation of amino acid positions on Rpn1 surface based on the phylogenetic relations between homologous sequences positioned on putative 3D conformation of Rpn1 from yeast as it appears in EM models of the 26S proteasome (using the ConSurf program and PDB:5A5B). Most highly conserved residues are painted dark red; least conserved positions are in light blue. The position of two nearest neighbors in the 19S, Rpt1 and Rpt2, are shown in light blue and green respectively according to the EM model. Most evolutionary conserved residues on the surface of Rpn1 contacted neighboring subunits Rpt1 and Rpt2. However, patches of conservation were identified on predicted solvent-exposed surfaces of the PC domain (e.g. residues painted dark red facing forward). **C. Protein interaction site on Rpn1 (NIPS).** A docking experiment with PyDock WEB server (Jimenez-Garcia et al., 2013) revealed a surface on Rpn1 with low-energy docking poses for complexes with monoUb. Normalized interface propensity (NIP) values derived from rigid body docking with electrostatics and desolvation scoring for the prediction of interaction hotspots. Rigid-body docking solutions generated by the simulations were subsequently used to project the docking energy landscapes onto full-length Rpn1 without any restraints. Most of the predicted hot-spot residues are above NIP values of 0.3. Even though possible interactions were not restricted to any region of Rpn1, the energetically preferred Ub docking poses mapped to the exposed region of the PC domain and to the hinge between the PC domain and the N-terminal extension of Rpn1 (Red). **D. Molecular docking analysis of ubiquitin docking onto Rpn1 structure.** Best 10 docking pyDockWEB results of Ub (PDB 1UBQ for ubiquitin ribbon, colored red) to Rpn1 (PDB 4CR2 for the Rpn1 structure, colored tan) suggested a specific association site on PC region covering residues ~350-640. Center of mass (spheres) of 100 best Ub-Rpn1 pyDockWEB results. Ten lowest energy Ub results are colored red showing location of center of mass and relative orientation to Rpn1 ribbon in tan. When performing docking of Ub on the PC domain structure, the 100 most preferred docking results distribute along the exposed edge of the PC ring particularly along the segment aa ~350-640 that encompasses the highly conserved hydrophobic residues (Figure 4G). Of these, the orientation of Ub docked at the ten most preferred sites fall into two clusters wedged between the circular PC repeat region and the extended N-terminus, in a solvent-exposed area of Rpn1.

A



B

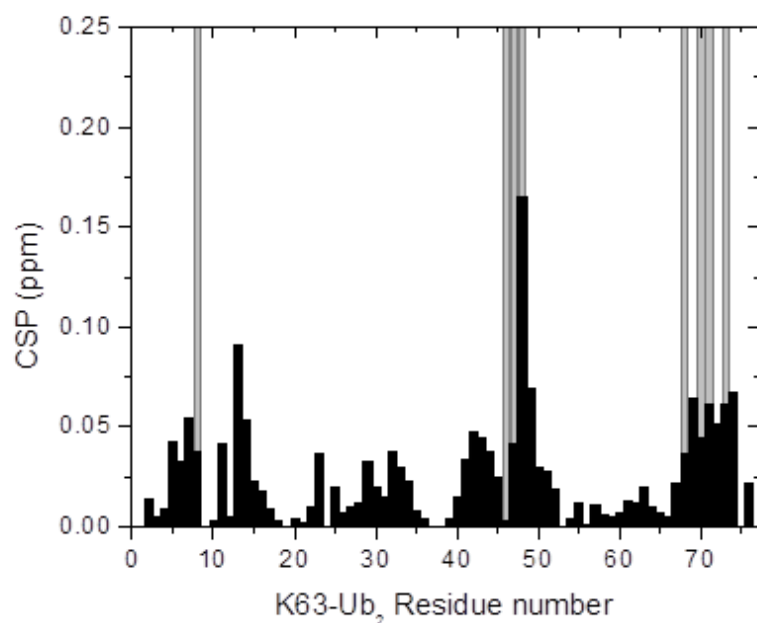


Supplemental Figure S4 - Rpn1 binds Ub via hydrophobic patch of Ub. Related to Figure 5.

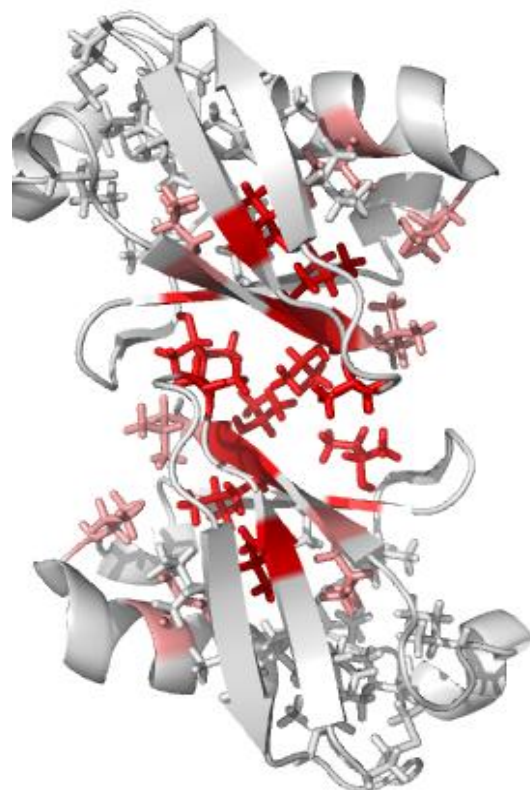
A. Site-directed mutagenesis confirms that recognition by Rpn1 involved hydrophobic patch of Ub. Mutations of the hydrophobic-patch residues L8 and I44 in Ub reduce Rpn1 binding. ¹⁵N transverse relaxation time (T_2) of backbone amides in WT Ub (black) and mutant (Ub^{L8A,I44A}) (blue) alone and in the presence of Rpn1³⁹¹⁻⁶⁴² at 1:1 molar ratio (red and green, respectively).

B. Predicted protein/protein interaction site on Ub and Rpn1^{PC}, NIPS. Normalized interface propensity (NIP) values derived from rigid body docking with electrostatics and desolvation scoring for the prediction of interaction hotspots. The ensembles of the rigid-body docking solutions generated by the simulations were subsequently used to project the docking energy landscapes mapping sites on Ub displaying preferable energy of interaction with Rpn1^{PC}. NIP values represent the frequency of a given residue to be located at the interface among the lowest energy solutions of docking points to Helices 586-590, 540-552 on the surface of Rpn1^{PC} upon interaction with free Ub as highly populated (dark green; left). The reciprocal experiment mapped sites on Ub displaying preferable energy of interaction with full-length Rpn1 picks out the hydrophobic patch of Ub and some neighboring residues (right). NIP values greater than 0.3 point to the canonical hydrophobic patch centered on L8, I44, and V70 (dark green) extending to some neighboring residues on one face of free Ub (light green, grey).

A



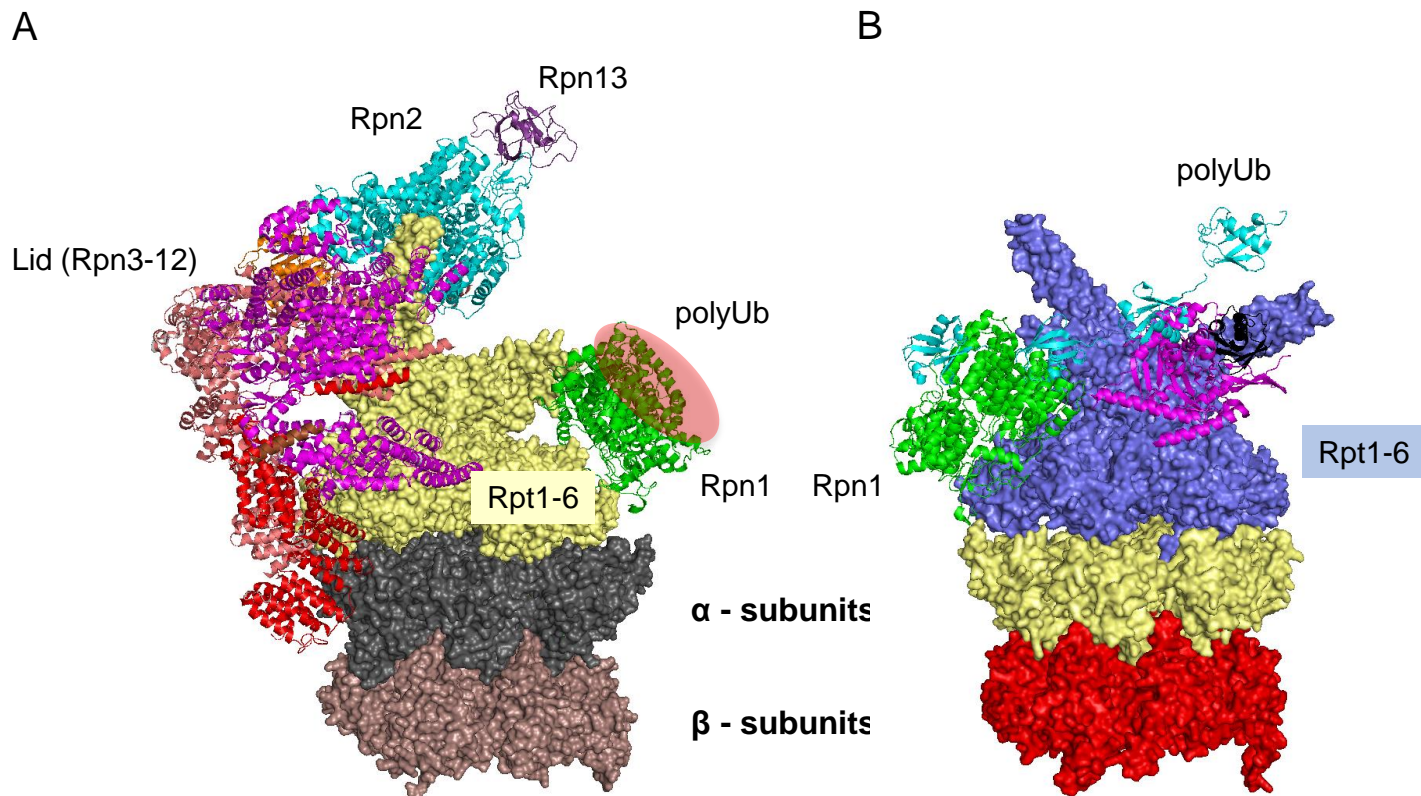
B



Supplemental Figure S5. Nature of association between Rpn1 and diUb. Related to Figure 6.

A. **NMR analysis of the binding interactions between Rpn1³⁹¹⁻⁶⁴² and K63-linked diUb.** Amide CSPs (black bars) in the distal Ub of K63-Ub₂ at the endpoint of titration with Rpn1³⁹¹⁻⁶⁴², as a function of residue number. Residues showing strong signal attenuations during the titration are marked with grey bars. Signal perturbations in K63-Ub₂ upon titration with Rpn1³⁹¹⁻⁶⁴² are similar to those in K48-Ub₂ (Figure 6).

B. **Interaction of K48-linked Ub₂ with Rpn1³⁹¹⁻⁶⁴² by Methyl TROSY.** Residues that shift upon addition of Rpn1 are colored according to the magnitude of CSP (red to white).



Supplemental Figure S6 – Model of how Rpn1 may position polyUb at 19S RP of proteasome for aiding substrate processing. Related to Figure 6.

(A) CryoEM model of the proteasome (PDB 5A5B) highlighting position of Rpn1 (green), and Rpn2-Rpn13 (cyan-purple) on the Six ATPases that make up the base of the 19S RP (Rpt1-6, as yellow surface). When incorporated into the proteasome, a wide swath of Rpn1 (encompassing the majority of its first PC stretch, rich in hydrophobic and conserved residues) does not contact other 19S subunits and is exposed to solvent. This region is positioned perfectly to concentrate proteasome auxiliary factors, proteasome-interaction proteins, and polyUb-conjugates at the entry point of proteasome entry (tan cloud). We suggest that through manifold protein-protein interactions, Rpn1 coordinates substrate recruitment and hand-over to proteasome-associated DUBs for chain removal and the substrate to RPT ATPases for unfolding and translocation. **(B)** Model demonstrating possible orientation of extended tetra-ubiquitin chain spanning Rpn1 (green) and Rpn11 (black) in the 26S proteasome. Proteasome EM model 5A5B was stripped of most lid and base 19S subunits to expose USP domain of Ubp6 (violet) and Rpn1 (green) in relation to RPT ring of ATPases (blue) situated on alpha (yellow) and beta (red) rings of 20S CP. Approximate size and orientation of extend tetra-ubiquitin chain (cyan) is superimposed to demonstrate that chains of three or longer Ub units are sufficient to tether UBA domains of shuttles or the USP domain of Ubp6/USP14 to Rpn1.